Volume: 2 Issue: 1 2021

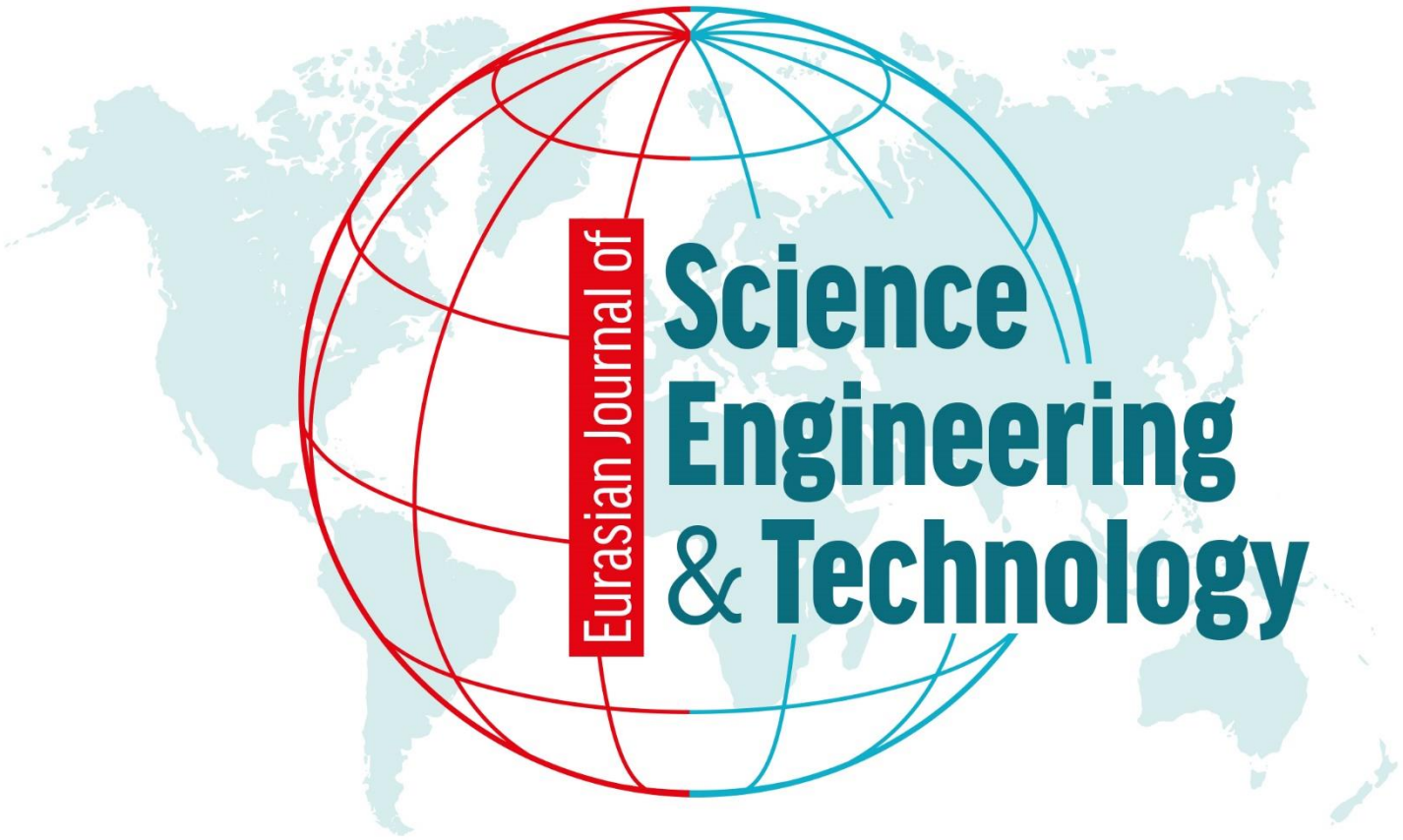

Eurasian Journal of Science Engineering and Technology

Editors

Editorial Board

Eurasian Journal of Science Engineering and Technology

Scientific Board

Eurasian Journal of Science Engineering and Technology

Correspondence Address

Niğde Ömer Halisdemir University
Eurasian Journal of Science Engineering and Technology Publishing Coordinatorship, 51240 Niğde/Turkey

***E-mail*:** recep.zan@ohu.edu.tr

***Web page*:** https://dergipark.org.tr/tr/pub/ejset

Publication information

The objective of Eurasian Journal of Science Engineering and Technology (EJSET) is to provide an academic environment for researchers in various fields of science and engineering and for the publication and dissemination of high-quality research results in the fields of science, applied science, engineering, architecture, agricultural science and technology.

Eurasian Journal of Science Engineering and Technology

İÇİNDEKİLER/*CONTENTS*

Eurasian Journal of Science Engineering and Technology

Research

DESIGN AND SIMULATION OF A HEAVY-DUTY VEHICLE STEERING COMPONENT BY ANALYTIC AND FEA METHOD

Mehmet Ziya OKUR [1,2], Durmuş Ali BİRCAN [2,*]

[1]*DİTAŞ Doğan Spare Parts and Manufacturing Inc., R&D Center, Niğde*
[2]*University of Çukurova, Faculty of Engineering, Department of Mechanical Engineering, Adana*

ABSTRACT

All vehicles need a steering system for safe driving. Drag link is a crucial component of the steering system in heavy commercial vehicles because it allows us to travel safely by transmitting the rotational movement from the arm of the pitman to the axle of the wheel linearly. The drag link used in a vehicle should be manufactured from materials that are resistant to variable loads depending on the vehicle's operating conditions. Furthermore, the rod arms must fulfill the expected function in tight spaces in the vehicle package data, and be designed in different bends and geometries depending on the regulation conditions they are subject to. In this study, different tube raw materials such as; St37-2, St 52-3, and P460 N were selected, and bending strengths calculated under various loading conditions. Finite Element (FE) models created, analyses performed, and the effects of different loads on the drag link were evaluated. Obtained results from the Finite Element Analysis (FEA) were compared with each other. Suitable material was selected based on analytic and FEA studies.

Keywords: Design of drag link, Finite element analysis, Buckling strength, Steering system.

1. INTRODUCTION

All vehicles must have the steering system for safe driving, as shown in Figure 1. Drag links, an essential component of the steering system in heavy commercial vehicles, are generally made up of hollow tubes with both ends connected by ball joints. They are critical for the vehicle to travel safely by transmitting the rotational movement from the pitman arm linearly to the axle of the wheel. The drag links used in a vehicle must be manufactured from materials resistant to variable loads coming from the vehicle, depending on the operating conditions. Furthermore, drag links are required to perform the expected function in narrow spaces in the vehicle package data and to be designed in different bends and geometries depending on the regulation requirements [1].

Drag link is produced by making different bends to the tube materials used in order to obtain the geometry suitable for the design. Usually, buckling failure may occur in these areas of the drag link due to different compressive loads occurring in road conditions. The buckling and deflection are also important parameters for the rod subjected to compression and tension due to the force based on the road [2].

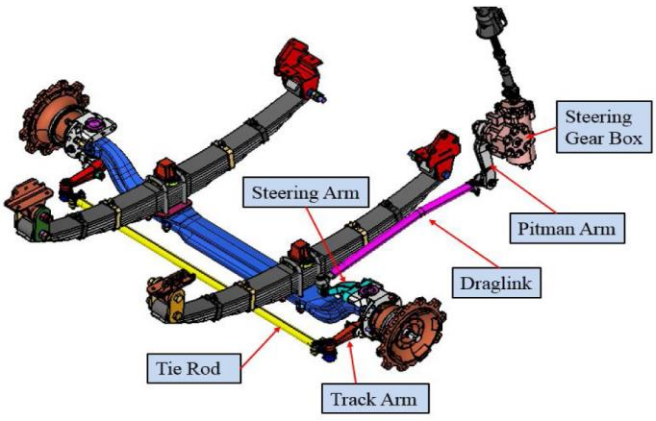

Figure 1. The schematic diagram for steering system & linkages [3]

*Corresponding author, e-mail: abircan@cu.edu.tr
Recieved: 03.06.2020 Accepted: 13.11.2020

This article is the extended version of the paper that was presented in the UTUFEM Conference 2019.

The buckling load calculation of the drag links as a critical part of driving system is crucial. Theoretical calculations take a long time due to the complex geometry of the rods in the design phase. On the other hand, verification tests performed to designed parts usually are costly and take a long time. Therefore, the Finite Element Method (FEM) used in determining the stresses and deformations to which the rods are exposed provides more accurate results in a short time [4]. Ganesh et al. (2014) studied the ford car steering rod's structural analysis and evaluated its performance [5]. Winklberger et al. (2018) studied on fatigue strength and weight optimization of the aircraft rods by using FEM. As a result of the study, it was determined that the tooth position had more effect on fatigue strength than tooth length [6]. Doke et al. (2016) calculated buckling strength for a drag link and analyzed its tubes against compressive loads. He also investigated the relations of various design parameters with buckling strength, which is useful for optimizing design parameters [7]. Kim et al. (2011) optimized the rod weight using the Al6082M aluminum alloy as a rod material [8].

Sener (2016) used road data collected from rods in order to be able to extract road characteristics. In his study, about 50 road routes and some rough road fatigue characteristics were acquitted with a Light Commercial Vehicle (LCV) equipped with sensors [9]. Neelakrishnan et al. (2017) analyzed the steering characteristics of an All-Terrain Vehicle (ATV) to improve the maneuverability of the vehicle by designed steering gearbox upright [10]. Gadher et al. (2017) studied the design and manufacturing of steering systems to acquire maximum Ackerman angles in the proposed steering system [11]. Aravind Kumar et al. (2016) designed to different types of drag links. They performed buckling analysis and rig tests to tube in a tube and typically designed drag links, results obtained from CAE and buckling test rig shows that the buckling load of the drag link can be improved by reinforcing the buckling zone [12]. Yaşar and Bircan (2015) examined optimum design parameters of the car chassis by taking into account different chassis types, dimensions, and materials to achieve minimum weight and deflection. They designed and analyzed for various geometries and materials. Also, they optimized the consequences of the analysis by the Taguchi method with Minitab. When studies are examined, FEM is used in applications such as weight and cost reduction, part optimization, and life predictions. It provides to take advantage of product development processes and design verification tests, also reduces cost by saving time and raw material [13, 14].

In this study, different tube materials made of ST37-2, ST52-3, and P460 N were described as calculation of buckling strength. Also, drag link tubes were analyzed in different compressive loads of 20, 25, and 40kN. The effects of various loading parameters on buckling strength were evaluated. Each value obtained from FEA results was compared. Analytical calculations were repeated to determine proper drag link for the design parameters.

2. MATERIAL AND METHOD

2.1. Design and Calculation of the Drag Link

The steering arm's buckling force is the force generated at the pitman arm's end because of turning forces in dynamic conditions, and equal to the exposed buckling load of the drag link tube. For the design of drag link against buckling loads, buckling strength must be more than the force generated at pitman arm end. The drag link used in a heavy vehicle can be illustrated in Figure 2.

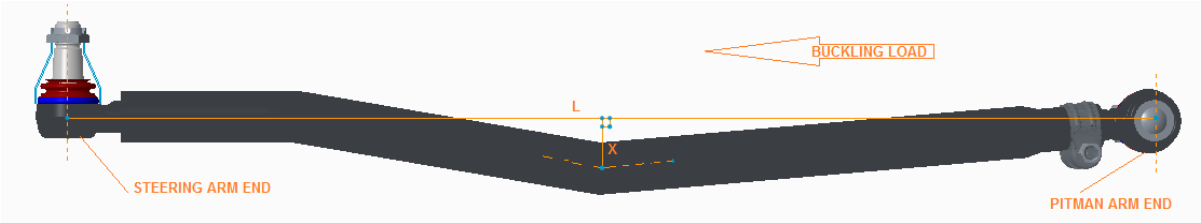

Figure 2. Buckling load on drag link tube

Crippling or Buckling Load (FB) can be expressed by using Rankine's formula for the drag link. It gives the ultimate load that the column can bear before failure. If the column is short (L<20D), the calculated load will be known as a crushing load. However, if L is longer than 20D (L>20D), the load will be buckling or crippling. The buckling formula is given in equation 1 (in case of long column):

$$F_B = \frac{(\sigma \times A)}{\left(1 + \frac{L^2}{6250 \times k^2} + \frac{(X \times Y)}{k^2}\right)} \quad (1)$$

Where σ refers to the yield strength of the tube material, changes depending on types of material, the radius of gyration (k) is defined as the distance from the axis of rotation to a point where the body's total mass is supposed to be concentrated, so the moment of inertia about the axis may remain the same. Simply, gyration is the distribution of the object; k is found as 15.70 mm. Moment of inertia (I) is the capacity of a cross-section to resist bending [15]. It is calculated as $204.442*10^3$ Kg-mm^4. Section modulus, Y is equal to 25 mm ($D_o/2$) and its area, A is 829.71 mm^2. Axis Height (X) is a distance between the centerline of the bent tube and the axis line drawn between the two end rods (L), as shown with the perpendicular line in Figure 2. L refers to the distance from center to center. The tube inner and outer diameter are illustrated as D_o and D_i, and these are 50 mm and 38 mm, respectively. They are critical for calculating the moment of inertia, its area, and section modulus. Offset of drag link tube, X is 59 mm. The design parameters of the tube structure used in the drag link were shown in Table 1.

The most critical parameter is the mechanical properties of the tube material when calculating buckling strength in the design of drag links. These tube materials are the most commonly used materials for drag link. Seamless tubes are preferred in automotive applications because of their durability. Buckling strength of tube materials are found by using Rankine's formula for drag link. St 37-2 seamless tube is one of the commonly used and cheapest tube materials on the market. However, it has about 30-35% lower mechanical strength than St 52-3 in terms of strength. The buckling strength of the St 37-2 seamless steel tube was calculated as 25.3 kN. Similar calculations performed for P460 N and St 52-3 seamless steel tube materials as 38.2 and 49.5 kN, respectively.

Table 1. Design parameters of tube structure used in drag link

Parameters	Unit	Value
Outer Diameter, D_o	(mm)	50
Inner Diameter, D_i	(mm)	38
Distance From Center to Center, L	(mm)	1059
Axis Height, X	(mm)	59
The radius of Gyration, K	(mm)	15.70
Moment of Inertia, I	(Kg-mm^4)	$204.442 * 10^3$
Section Modulus, Y	(mm)	25
Area, A	(mm^2)	829.71
Calculated Buckling Strength	(kN)	25.3 For St 37-2 38.2 For St 52-3 49.5 For P 460 N

Tube materials of the drag links exhibit different properties and mechanical performance depending on the amounts of their chemical composition. In particular, elements such as C and Mn in the structure of steels directly affect the strength of the structure. Chemical compositions of tube materials used in the study are given in Table 2.

Table 2. Chemical compositions for tube materials

Content (%)	St37-2	St52-3	P460 N
C	0.17	0.22	0.20
Si	0.35	0.55	0.60
Mn	1.40	1.60	1.70
P	0.05	0.05	0.03
S	0.05	0.05	0.042

Seamless tube material of St 52-3 does not meet the target strength values in the drag link design, P460 N tube material may be preferred. This material has 1.3 times higher strength than St 52-3 tube material. However, it affects product costs significantly since it is much more expensive than St 37-2 and St 52-3 tube materials. The mechanical properties of tube materials are tabulated in Table 3.

Table 3. Mechanical Properties of Tube Materials

Mechanical Properties	St 37-2	St 52-3	P460 N
Tensile Strength (MPa)	460	570	680
Elongation at Fracture (%)	25	21	19
Yield Strength (MPa)	235	355	460

3. ANALYSIS OF BUCKLING STRENGTH FOR DRAG LINK

When the solid model is to be analyzed by using the FEM, the model is simplified by removing the assembly parts, which can not affect the result of the analysis. In this way, the solution time of the mathematical model is decreased. In the analysis, drag links with three different tube materials as St 37-2, St 52-3, and P460 N were compared. Proper meshing operation on geometry is an essential parameter for reducing errors in numerical calculations. For the geometries that evaluated in this study, tetrahedral elements performed better results and reduced mathematical error. The drag link's structural meshing can be seen in figure 3. After the properties were assigned and mesh operation was performed, the boundary condition of the drag link was applied as fixing from one of the housings and 40, 25, 20 kN compressive load from the other.

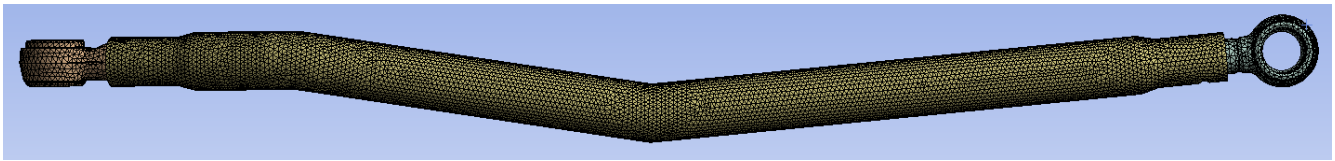

Figure 3. The structural meshing of the drag link

On the other hand, mesh dependency is very critical in FEA. Therefore, the simulations are repeated for different mesh densities for St52. The properties of the mesh and the resulting maximum stresses are calculated by changing the mesh sizes iteratively. Convergence and mesh independence for FEA is given in Table 4. The element quality and deviation values decrease as the mesh size decreases. Furthermore, element quality is increased by decreasing the mesh size and at the maximum for 4 mm mesh size. Decreasing the mesh size to less than 4 mm increases the number of elements and changes the observed maximum stress negligibly. The change in the maximum stress according to the number of elements is plotted based on the values in table 4. Mesh independence is shown in Figure 4 with the graph of maximum stress – number of element in mesh. Adding elements increases the solving time. At some point, more items with without improvement in the solution increase the solution time. The improvement made after this point is an inefficient implementation of FEA.

Table 4. Convergence & Mesh Independence for FEA

Mesh Size (mm)	Max. Stress (MPA)	Number of Nodes	Number of Elements	Element Quality (Average)	Standard Deviation (%)
20	329.03	40291	24055	0,71326	0,20608
15	346,95	43750	25774	0,72106	0,19294
10	356,4	53484	30629	0,75161	0,17832
5	368,89	149109	88759	0,79044	0,13503
4	370,76	223574	134477	0,83192	0,12179
3	373,74	445132	278533	0,80673	0,11471
2	377,79	1341250	887613	0,8261	0,1024

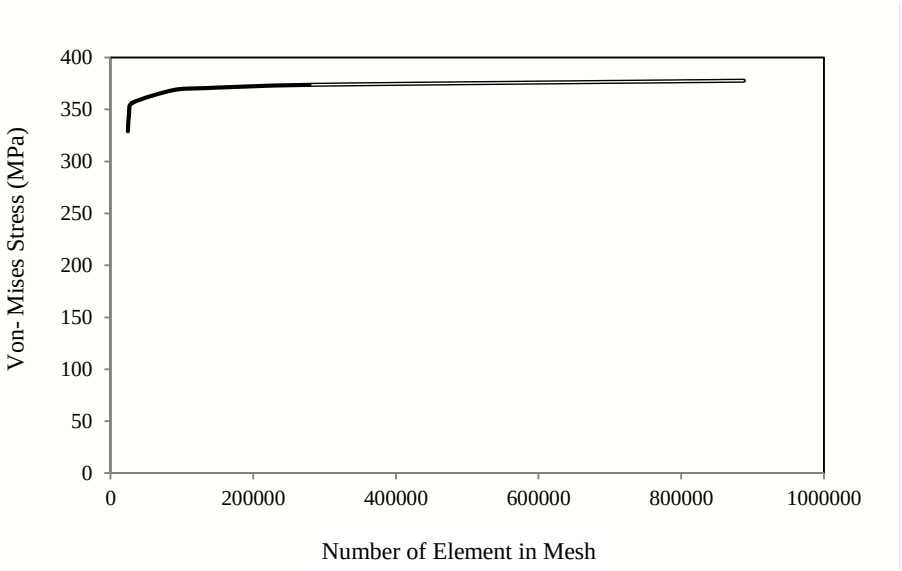

Figure 4. The maximum stress-number of element in mesh

4. RESULTS AND DISCUSSION

The drag link, a steering part of a heavy commercial vehicle, was designed using 3D parametric software Creo 3.0, and the analyses were conducted using ANSYS via the FEA method. The development and application of the FEA considerably reduce the time and effort required for the steering components design process [16]. Designed drag link geometry was evaluated by defined raw materials of the tube with different loads. The maximum buckling load that the tube material can withstand is found by calculating the buckling strength. The maximum buckling load refers to the load value that the drag link can withstand without plastic deformation. As a result, the stress at the bending point of the tube for 40 kN load is close to the yield point of the St 52-3. Therefore, proposed drag link should be made by P 460 N has higher buckling strength for compressive loading 40 kN and more. Because, loading 40 kN or more is risky for St 52 tube material, and loadings over than 38.2 kN exceed to elastic limit of the St 52-3 tube material. On the other hand, St 37-2 tube material is unsafe for over 25 kN loading. Design calculations and FEA provide an advantage in material selection and product costs. The drag link should be designed with the optimum material by considering the loads which are exposed to.

For loading 40 kN, Von-Mises stress distributions of St 37-2, St 52-3, and P460 N tubes were illustrated in Figures 4, 5, 6 and 7, respectively. Stress concentration on tube has occurred at tube bending areas as expected. 377.4 MPa was calculated as highest Von-Mises stress on the geometry, and 1.218 was found as a minimum safety factor for P460 N. Also, 360.81 MPa was calculated as highest Von-Mises stress on the geometry, and 0,983 was found as a minimum safety factor for St 52-3. The stress at the bending point of the St 52 tube under 40 kN load is over its yield point. Therefore, this load is critical for St 52 tube material. Also, the St 37-2 material is completely deformed at this loading, which is 55% higher than the bending strength calculated, and St 37-2 is not recommended for a drag link with such geometry. Von-Mises stress occurred on St 37-2 is 359.52 MPa, and safety factor is 0.653. Both tube materials have similar stress values for the same loading conditions. This shows that this drag link should be made by P 460 N, has higher buckling strength for 40 kN compressive loading.

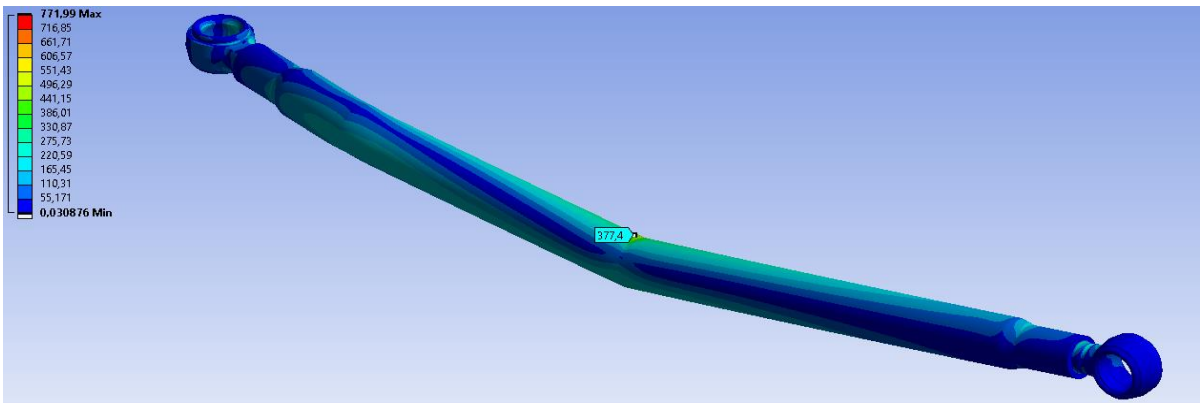

Figure 4. Stress Distribution of the P460 N Tube for 40 kN (Von-Mises)

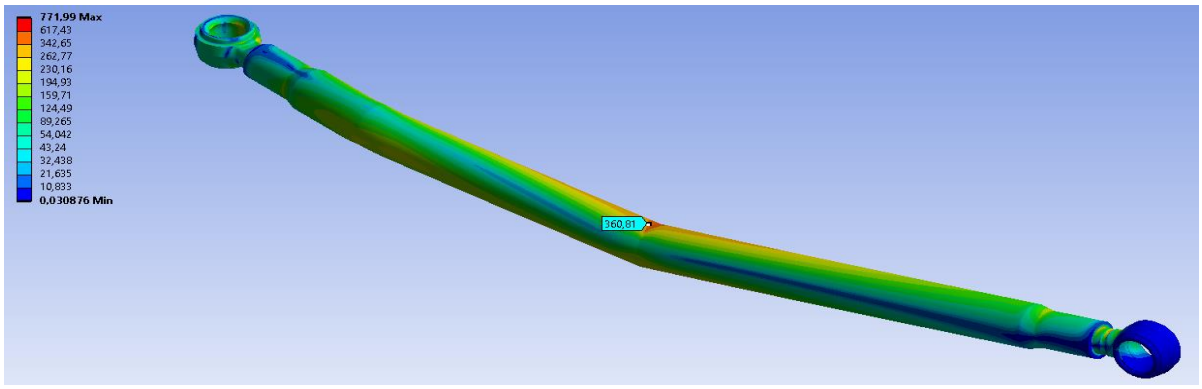

Figure 5. Stress Distribution of the St 52-3 Tube for 40 kN (Von-Mises)

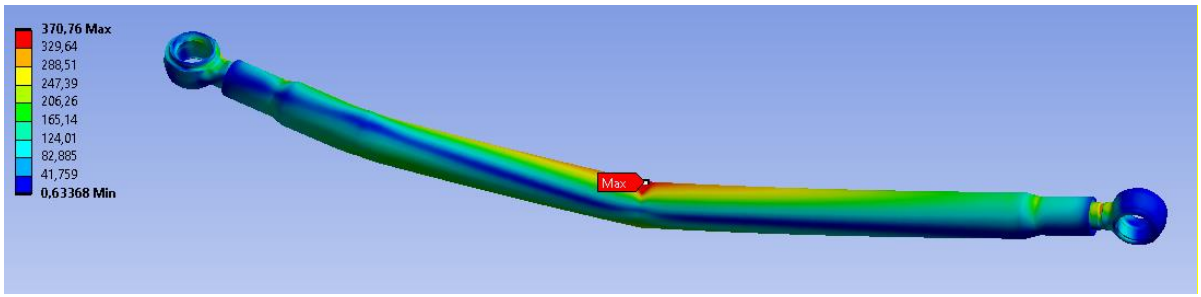

Figure 6. Stress Distribution of the St 52-3 Tube for 40 kN (Von-Mises) (mesh size 4 mm)

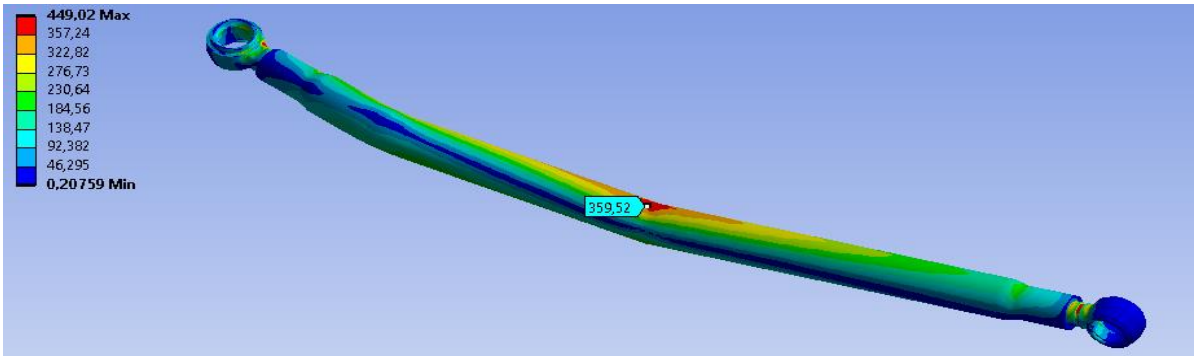

Figure 7. Stress Distribution of the St 37-2 Tube for 40 kN (Von-Mises)

The highest stress for 40 kN load were seen as 771.99 MPa when the stress distribution obtained from the analysis examined. However, sudden stress increases were observed in some mesh elements. This is called the singularity. In the analysis, the critical stresses are occurred on the tube bended region, these stresses due to singularity are ignored.

In addition, the mesh independence was studied and the analysis was repeated for the st52-3 tube material. Stress distribution of the St 52-3 Tube for 40 KN was shown in Figure 6. With the improvement of the mesh size and properties, singularities were eliminated, and the maximum stress was observed again in the tube bended region. In the repeated analysis, very little change was observed in the maximum stress value of the tube material and this difference of approximately 2.8% was neglected as it would not significantly change the overall results.

For loading 25 kN, analyses of St 37-2, St 52-3, and P460 N tubes were performed and von-Mises stress distributions were investigated. The stress concentration for 25 kN is approximately 35% lower than 40 kN, and 2.067 was found as a minimum safety factor for P460 N. Also, similar Von-Mises stress on the geometry and 1.532 was found as a minimum safety factor for St 52-3. This stress at the bending point is not critical, and also both of these tube materials are safe for 25 kN compressive loading. Stress concentration on St 37 was calculated as 232.12 MPA. It is close to its yield strength, and the minimum safety factor for St 37 was calculated as 1.012. Therefore, 25 kN loading is safe for all raw material, but St 37-2 tube material is unsafe if 25 kN loading is exceeded for proposed design.

As a result of the analyses carried out for 20 kN tubing materials, von- Mises stress on the part decreased depending on the loading. For loading 20 kN, Von-Mises stress distributions of drag links produced with P460 N, St 52-3, and St 37-2 tube materials were obtained similar to other loadings. The stress concentration decreased by 50% compared to the initial loading (40 kN) due to the reduction of the load. Minimum safety factors for P460 N, St 52-3, and St 37-2 were found as 2.486, 1.936, and 1.197. Stress occurred at the bending point is not critical, and all of these materials are safe for 20 kN compressive loading. If one of these three materials is preferred for the 20 kN loading value, safe drag link designs with 1.2 safety coefficient desired from the steering system parts can be realized. In Figure 8, Von-Mises stress-force and safety factor of the tube materials are seen comparatively.

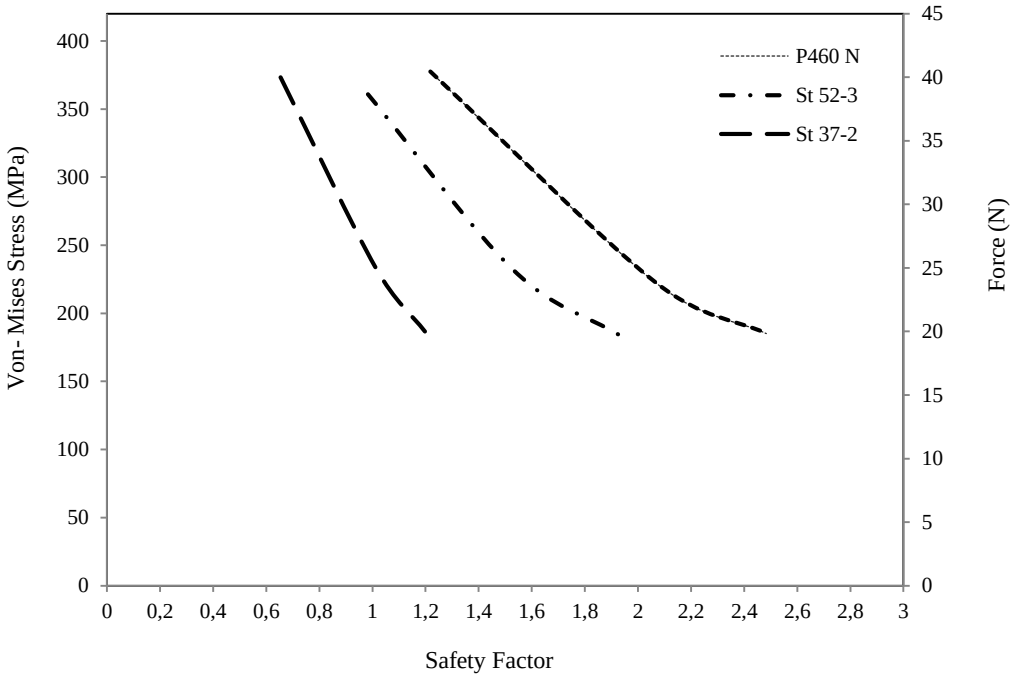

Figure 8. Von-Mises Stress-Force and Safety Factor of the tube materials

Analytical calculations are carried out for the drag link and the total stresses in the part are calculated from the normal stress and bending stresses. Theoretically calculated stress values for geometry of drag link are 183, 229 and 366 MPA for 20, 25 and 40 KN, respectively. Comparison of analytical calculations and FEA results was given in Table 5. When these calculations are examined, the calculated and analysis results match each other. Generally, error rates are mostly in the range of 0,21-3,75%, and FEA results with an error of less than 5% are acceptable.

Table 5. Comparison of Analytical Calculations and FEA Results

Tube Material	Loading (KN)	Calculated Theoretical Stress (MPA)	FEA results (MPA)	Error (%)
St 37-2	40	366,16	359,52	1,81
St 52-3	40	366,16	370,76	1,25
P460 N	40	366,16	377,4	3,06
St 37-2	25	228,85	232,12	1,42
St 52-3	25	228,85	223,69	2,25
P460 N	25	228,85	220,26	3,75
St 37-2	20	183,08	179,80	1,79
St 52-3	20	183,08	177,22	3,20
P460 N	20	183,08	183,47	0,21

5. CONCLUSION

In this study, the buckling strength of proposed drag link in a heavy vehicle for different tube materials of P460 N, St 52-3, and St 37-2 was calculated analytically. The effects of various bending parameters on buckling strength were evaluated. It was suggested that the drag link should be made by P 460 N, with higher buckling strength, compressive loading 40 kN, and more.

20, 25, and 40 kN compressive loads were applied to the drag link model in FEA. The stress at the bending point of the tube for 40 kN load is close to the yield point of the St 52. Therefore, designed drag link should be made by P 460 N, which has higher buckling strength for compressive loading 40 kN and more. Because, loading 40 kN or more is risky for St 52 material, and loadings over than 38.2 kN exceed to elastic limits of the tube material. All suggested materials are safe for 20 and 25 kN loading, but St 37 material should not be selected for loadings over 25 kN. If one of these materials is preferred for the 20 kN loading based on light duty vehicles, safe drag link designs with 1.2 safety factor desired. Consequently, the material should be selected taking into account the criteria of reliability and affordability for a drag link (or another steering component) with optimum performance in a heavy-duty vehicle.

REFERENCES

[1] G. F. T. Möller, "The Noise and Vibration Transfer Characteristics of the Steering Installation in a Volvo FH Truck", M. S. thesis, Chalmers University of Technology Gothenburg, Sweden. 2015.

[2] M. A. Patil, D. S. Chavan, M. V. Kavade, and S. Ghorpade, ''FEA of Tie Rod of Steering System of Car'', *International Journal of Application or Innovation in Engineering & Management*, vol. 2, pp. 222-227, 2013.

[3] S. Kurna, S. Jain, P. Raja, and L. Vishwakarma, ''Truck Steering Component and Linkages Analysis Using Finite Element Method'', SAE Technical Paper 2017-01-1478, 2017.

[4] E. Uludamar, S. G Biçer, and M. Taş, ''Sonlu elemanlar metodu kullanılarak rot üzerinde oluşan gerilmelerin hesaplanması.'' *Adana Bilim ve Teknoloji Üniversitesi Fen Bilimleri Dergisi*. vol. 1, no. 2, pp. 30-35, 2018.

[5] M. S. Ganesh, B. Patil and N.A. Kharche N. A., ''Performance of the Structural Analysis of Ford Car Steering Rod''. *International Journal of Research in Advent Technology*, vol. 2, no. 2, pp. 1-5, 2014.

[6] M. Winklberger, P. Heftberger, M. Sattlecker and M. Schagerl, ''Fatigue strength and weight optimization of threaded connections in tie-rods for aircraft structures'', *Procedia Engineering*, vol. 213, pp. 374-382, 2018.

[7] Y.N. Doke and S. M. Shaikh, ''Design & Analysis of Steering System Drag Link Against Buckling Loads For Tipper Application'', *International Journal of Innovations in Engineering Research And Technology* [IJIERT], Issn: 2394-3696, 2016.

[8] J. K. Kim, Y. J. Kim, W. H Yang, Y. C. Park, and K.H. Lee, ''Structural Design of an Outer Tie Rod for a Passenger Car'', *International Journal of Automotive Technology*, vol. 12, pp.375- 381, 2011.

[9] A. S. Sener, ''Steering Wheel Tie Rod Fatigue Life Determination According to Turkish Mission Profiles'', *International Journal of Engineering Technologies*, vol. 2, pp. 56-63, 2016.

[10] S. Neelakrishnan, T. Kowshik, G. Krishnakuma and M.P. Bharathi Mohan, ''Analysis and Improvement of the Steering Characteristics of an ATV'', *Int. Journal of Engineering Research and Application*, vol. 7, no. 5, pp.18-25, 2017.

[11] H. Gadher, T. Patel, C. Modi and Z. Bhojani, ''Design and Optimization of Steering System'', *International Research Journal of Engineering and Technology (IRJET)* e-ISSN: 2395-0056 vol. 4, no. 10, 2017.

[12] K. H. Aravind Kumar, A. Vijayanand and S. Arul Selvan, ''Design Optimisation and Buckling Analysis of Tube in Tube Drag Link'', *Int. J. Chem. Sci*. vol. 14, pp. 543-548, 2016.

[13] A. Yaşar and D. A. Bircan, ‘‘The Influence of Different Design Parameters by means of Analysis and Optimization in a Car Chassis’’, *International Journal of Natural and Engineering Sciences*, vol. 9, no. 2, pp. 1307-1149, 2015.
[14] A Yasar and D.A. Bircan, “Design, Analysis and Optimization of Heavy Vehicle Chassis Using Finite Element Analysis”, *International Journal of Scientific and Technological Research*, ISSN 2422-8702, vol. 1, no. 6, 2015.
[15] R. G. Budynas, J. K. Nisbett, and J. E. Shigley, Shigley's mechanical engineering design. New York: McGraw-Hill, 2011.
[16] D.A. Bircan, K. Selvi, A. Ertaş and A. Yaltırık, “Design and Analysis of Electrically Operated Golf Cart Chassis Using FEA”, *Çukurova University Journal of the Faculty of Engineering and Architecture*, vol. 30 no.1, pp. 87-94, 2015.

Eurasian Journal of Science Engineering and Technology

Research

INVESTIGATION OF THE EFFECT OF HEATING RAMPING RATE ON Cu(In, Ga)Te_2 THIN FILMS

Serkan ERKAN[1,*], Yavuz ATASOY[2], Ali ÇİRİŞ[3], Emin BACAKSIZ[4]

1,2,3 Niğde Ömer Halisdemir University, Nanotechnology Application and Research Center, 51240 Niğde
2. Niğde Ömer Halisdemir University, Niğde Zübeyde Hanım Health Services Vocational High School, 51240 Niğde
4. Karadeniz Teknik University, Faculty of Science, Department of Physics, 61080 Trabzon

ABSTRACT

Cu(In,Ga)Te_2 (CIGT) thin films were grown using a two-stage method. In the first stage, (Cu, In, Ga) precursor layers were grown on Mo coated flexible stainless steel substrates using the electro-deposition method. NaF and Te layers were grown on metallic precursor layers using electron beam evaporation method. In the second stage, the foil/Mo/(Cu, In, Ga)/NaF/Te stacks were reacted at 600°C for 5 minutes by rapid thermal processing. The temperature ramping rates in this procedure were 0.5°C/sec, 1°C/sec, 5°C/sec and 10°C/sec. In order to investigate the effect of temperature ramping rate on the structural properties of CIGT thin films, XRD, Raman, SEM and EDS measurements were performed. Regardless of the ramping rates, it was determined that all samples crystallized in chalcopyrite structure. According to the Raman spectra, as the ramping rate increased, position of the A_1 mode completely changed and shifted from 127 cm^{-1} to 135 cm^{-1} due to bond-stretching forces between the nearest-neighbor atoms. It was concluded that CIGT thin film reacted with a ramping rate of 5°C/sec had superior properties compared to other samples.

Keywords: Cu(In,Ga)Te_2, Heating ramping rate, Two-stage process, Electro-deposition

1. INTRODUCTION

Ternary and quaternary absorber layers such as Cu(In)$(S,Se,Te)_2$ [1-4], Cu(Ga)$(S,Se,Te)_2$ [5-7] and Cu(In,Ga)$(S,Se,Te)_2$ [8-11] which are consisting of elements of the I-III-VI_2 group have an important potential in photovoltaic (PV) applications. In addition, the small area Cu(In,Ga)$(S,Se)_2$ (CIGSSe) cells were reported to have a photo-conversion efficiencies of over 22% [12, 13]. These compounds that crystallize in chalcopyrite structure have high optical absorption coefficient (>10^4 cm^{-1}) and direct transition band structure. In addition to these features, the band gap of this absorber material is adjusted by altering the compositions of the constituent elements. For example, the band gap of CIGSSe varies between 1.00 eV to 1.72 eV depending on the amount of Ga and/or S in the compound [14]. Similarly, the band gap of the Cu(In,Ga)Te_2 (CIGT) compound varies in the range of 0.96 eV ($CuInTe_2$) -1.35 eV ($CuGaTe_2$) [15].

There have been many studies focusing on changing the amount of Ga in place of In in the CIGSSe thin films. In one of these studies, Cu(In,Ga)Se_2 (CIGS) thin films were produced using a two-step method with the goal of varying the atomic ratios of [(Ga)]/[(Ga)+(In)]. In the grown samples, it was seen that Ga was inhomogeneously distributed through thickness of the film, accumulated near to Mo-back contact and had Se-rich of the film surface. This distribution of the Ga causes the formation of compositional non-uniformity resulting SLG/Mo/CGS/CIS type structure which reduces solar cell efficiency. However, it was found that the diffusion of Ga towards the surface of the film became easier with the increase of the annealing temperature (≥575ºC) [16]. To investigate the effect of Cu content on the structural properties such as phase evaluation and crystallinity of the CIGS thin films, Witte et al. produced CIGS thin films with various amount of Cu by an in-line co-evaporation process. According to the Raman spectra of the samples, it was observed that A_1 modes shifted to low values with increasing Cu content. Furthermore, the full width at half maximum (FWHM) values of the A_1 mode decreases with increasing Cu content, due to the better crystallinity and reduced disorder in the films [17]. Rudmann et al. prepared CIGS layers using DC sputtering on Mo coated soda-lime glass substrates (SLG) to investigate the impact of Na diffusion on the properties of CIGS. According to scanning electron microscope (SEM) images, they observed a reduction in grain size of the films in the presence of Na during growth [18]. However, the studies on telluride quaternary compounds are quite limited. Gremenok et al. produced the

*Corresponding Autor: e-mail: srknerkan25@gmail.com
Recieved: 07.05.2021 Accepted: 27.05.2021

$CuGa_xIn_{1-x}Te_2$ thin films by changing the amount of Ga. As a result of the X-ray diffraction (XRD) analysis, it was seen that thin films crystallized in chalcopyrite structure, with a preferential orientation along (112). They revealed that the lattice parameters and band gaps of the samples changed linearly with the amount of Ga [19]. Sanad et al. produced CIGT thin films with micron and sub-micron thicknesses using a simple co-precipitation method to get high-performance photogene materials in PEC solar cell devices. They observed that crystallographic and morphological properties can be easily controlled by changing the In^{3+}/Ga^{3+} molar ratio [20]. Gaburicci et al. reported on polycrystalline bulk $CuIn_{1-x}Ga_xTe$ samples with the different atomic ratios of 'x' (x= 0 - 1) by using rapid cooling technique. XRD measurements have shown that all samples crystallized in chalcopyrite structure, however In_2Te_3 secondary phase formed. They reported that the rapid cooling technique is very suitable for indium-rich compounds, but not for gallium-rich compounds [21]. In another study, Rincon et al. examined the relationship between Urbach energy and temperature for $CuInTe_2$ compound. The vibration modes of chalcopyrite structures of different compounds such as $CuGa_3Te_5$, $CuIn_3Te_5$, $CuIn_5Te_8$ were also examined by the same research group [22-26].

In this study, CIGT thin films were grown using a two-step method. In the first stage, (Cu, In, Ga) metallic precursors were grown by electro-deposition method followed by Te and NaF layers were evaporated over the metallic precursors using electron beam system. In the second stage, the resultant layered-structures were reacted with different ramping rates at the targeted temperature by rapid thermal processing (RTP). The effect of different ramping rates on the structural properties of CIGT samples are examined in detail.

2. MATERIAL AND METHOD

CIGT samples were produced using a two-stage method. In the first stage of the method, Cu-In-Ga metallic layers were deposited on the Mo coated 304 stainless steel foil by using an electro-deposition system. Detailed information about the electro-deposition of Cu, In, Ga layers are found in previous studies [15, 27]. The thickness of the Cu, In and Ga films grown by electro-deposition method were determined individually by counting the loads passed on the stainless-steel substrate [23]. The thickness of stainless steel foil and Mo back contact layer is 50 μm and 1.5 μm, respectively. Theoretical and experimental studies on CIG(S,Se) thin films produced with different atomic ratios show that the best solar cell efficiency value is obtained from Cu-poor and low Ga-doped absorption layers [13]. Therefore, the stoichiometric ratio determined for metallic layers is about 0.3 for [Ga]/([Ga]+[In]) and 0.7-0.9 for [Cu]/[In]+[Ga]). The nominal thickness of Cu-In-Ga layers corresponding to these ratios were determined as 160, 270 and 90nm, respectively. NaF (3N) [25] and Te (5N) layers were evaporated over the Cu-In-Ga layers using with electron beam system. In the second stage, (Cu, In, Ga)/NaF/Te stacks were thermally annealed in an RTP furnace. The ramping rates of 0.5, 1, 5 and 10 °C/sec were employed for annealing process. Annealing process was carried out in Ar atmosphere, at the target temperature of 600°C for 5 minutes. Heat treatment of the samples was performed in RTP furnace.

XRD measurements of the samples were performed in the range of $2\theta = 20°–70°$ using the Rigaku SmartLab unit ($\lambda = 1{,}5405$ Å) with CuKα source at room temperature. Raman spectra were obtained with the Renishaw-INVI Reflex Confocal Raman System using a 532 nm laser excitation source at room temperature. SEM images were taken with JEOL JSM 6610 scanning electron microscope. The compositions of the growth films were determined using Oxford Instruments Inca X-act EDS Analysis Unit.

3. RESULTS AND DISCUSSION

3.1. X-Ray Diffraction (XRD) Spectra

XRD spectra of CIGT thin films reacted with different ramping rates are shown in Figure 1. In addition, 2θ diffraction angles and d-spacing values of the main peak are given in Table 1. When the figure and table were examined, it was seen that all samples crystallized in chalcopyrite structure irrespective of the ramping rates. All characteristic peaks of the chalcopyrite structure (112), (220/024) and (312/116) were observed in diffraction patterns of all samples (JCPDS Card No: 00-049-1326) [28]. Besides, it was determined that peaks appeared at $2\theta = 40.5°$ and 58.5° are associated with the Mo back contact (JCPDS Card No: 00-042-1120). As can be seen in Table 1, the 'd' values corresponding to the peak positions (112) are in the range of 3.53-3.55 Å for all samples. The lattice parameter 'a' corresponding to these d-values were also calculated using Equation 1 [29],

$$a = \left(\frac{d}{2}\right)\sqrt{4\left(h^2 + k^2\right) + l^2} \quad (1)$$

where (h, k, l) are Miller indices. For tetragonal structures, these indices are h =1, k = 1 and l = 2. In addition, the crystallite sizes of the samples were calculated with the Scherer formula in Equation 2 [30, 31].

$$D_{(h,k,l)} = \frac{0.9\lambda}{\beta \cos\theta} \quad (2)$$

where λ is the X-ray wavelength, β is the FWHM of (112) peak and θ is the diffraction angle. The calculated values by using Equation 2 were given in Table 1. It was observed that the samples reacted with 0.5, 1 and 10 °C/sec had high FWHM values, indicates the samples may consist of compounds with different Ga-gradients throughout the thin film. In a recent study, the Ga distribution of CIGT films produced using a two-stage method was examined by angle dependent-XRD analysis. It was confirmed that the films represent a series of Ga compositions throughout the layer, resulting in higher Ga content near the back contact [25, 32].

According to the XRD spectra of our samples, it was observed that the (112) peak intensity increased with the increase ramping rate, reached maximum value for the sample reacted with 5°C/sec, then decreased again with the increment of the ramping rate. In addition to this, sample reacted with 5°C/sec has the lowest FWHM value (0.18°) and a sharper peak. Within this context, the best crystallization was shown in the sample reacted with ramping rate of 5 °C/sec.

It was concluded that no secondary phases were observed in all samples regardless of the ramping rate. The formation of a single phase structure indicates that the dwell time used in the process is sufficient [25]. On the other hand, in the last column of the Table 1, the ratio of the Mo to CIGT main peak intensities (I_{Mo}/I_{CIGT}) is given. Although Mo peak intensity is the lowest for 10 °C/sec, the ratio of I_{Mo}/I_{CIGT} is the highest value. For the samples reacted with 0.5, 1 and 5°C/sec, the ratio of I_{Mo}/I_{CIGT} varied in the range of 0.38-0.40.

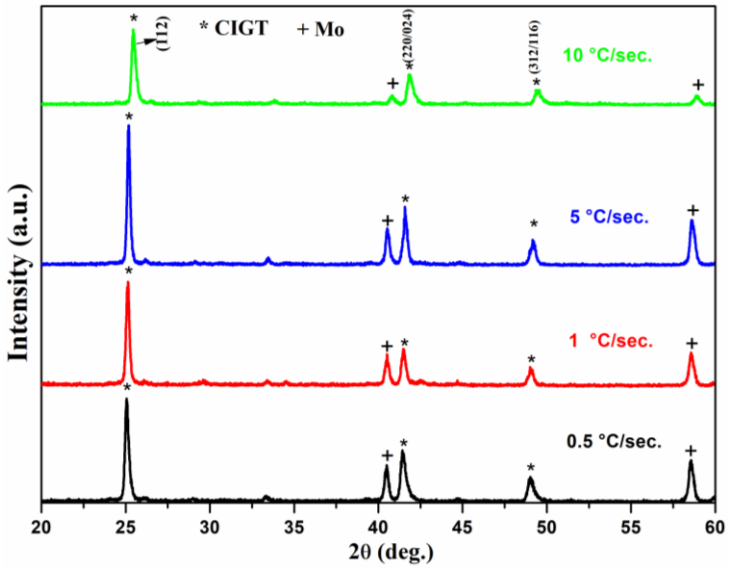

Figure 1 XRD spectra of CIGT thin films reacted with different ramping rates

Table 1 Some structural parameters calculated based on (112) main peak in the XRD spectra

Ramping rate (°C/sec)	2θ (°)	d (Å)	a (Å)	β_{FWHM} (°)	Crystal size (nm)	$I_{Mo}/I_{(112)}$
0.5	25.05	3.55	6.15	0.24	34.04	0.38
1	25.07	3.54	6.14	0.23	35.87	0.40
5	25.11	3.54	6.13	0.18	43.16	0.39
10	25.20	3.53	6.12	0.22	36.39	0.46

3.2. Raman Spectra

Raman spectra of CIGT films reacted with the ramping rates are given in Figure 2. The Raman shifts and corresponding of the Raman modes of our samples and their related reference values are given in Table 2. As can be seen in Figure 2, Raman peaks were observed at 106, 117, 128 and 170 cm^{-1} for the lowest ramping rate (0.5 °C/sec). These peaks are attributed to B_2^2, B_1^2, A_1 and E^5 or B_2^3 vibrational modes, respectively [25]. The dominant A_1 mode located at 128 cm^{-1} depends on the planar motion of the cation and anion (tellurium) atoms. Also, large-shaped phonon frequencies around 200 cm^{-1} may be attributed to the combination of E and B_2 modes [26]. These peaks seen in the Raman spectra are consistent with the reported values in previous studies [23-26].

In Raman spectra, it was seen that there were small shifts in the peak positions with the ramping rate in the range of 0.5-5°C/sec. However, the Raman spectrum of 10°C/sec was completely changed. This change can be clearly seen in the inset of Figure 2, which demonstrates the expanded form of A_1 modes in the spectra. Besides, when the ramping rate is increased from 0.5 to 1°C/sec, there is a slight shift in the main peak and a new shoulder appeared next to the main peak. The resulting phase separation indicates different Ga compositions through the film, as stated in the XRD section. It shows that this phase has changed completely from CIGT to CGT with shifting of the main peak from 127 cm^{-1} to 135 cm^{-} for the sample reacted with 10°C/sec. This situation may result from the changing of the surface morphology, the deviation of film stoichiometry (especially Ga amount) or bond stretching forces between the nearest-neighbor atoms [33, 34].

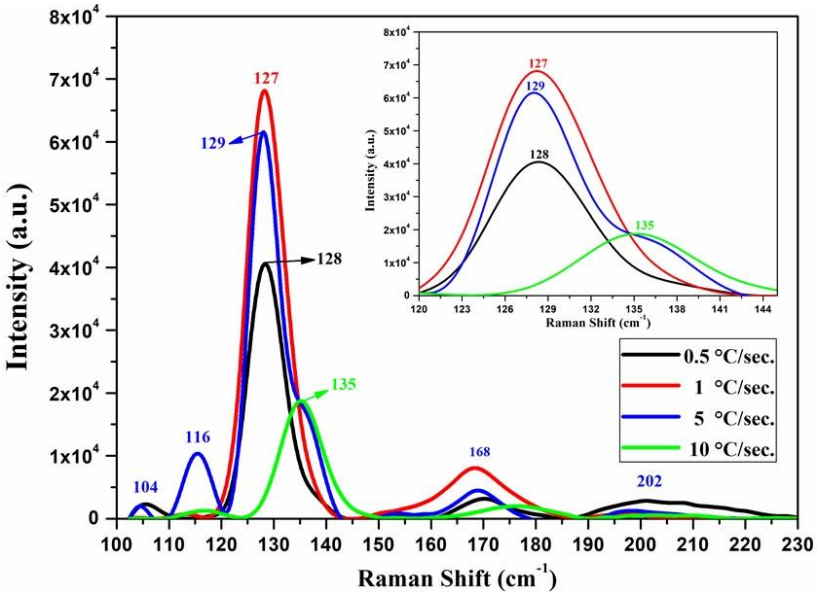

Figure 2 Raman spectra of CIGT thin films reacted with different ramping rates

Table 2 . The peak positions observed and the reference values for the Raman modes

0.5°C/sec.	1°C/sec.	5°C/sec.	10°C/sec.	CIT (Ref.)	CGT (Ref.)
106	104	104	104	106[a] [B_2^2]	-
117	114	116	117	116[a] [B_1^2]	117[c],122[b] [A_2]
128	127	129	-	125[a] [A_1]	-
-	-	135	135	-	136[b], 138[c] [A_1]
-	168	168	-	162[a] [E_1^4]	-
170	-	-	177	170[a][E_1^5], [B_2^3]	173[b], 185[b] [B_2-E]
200	202	202	202	192[a][E_1^6]	205[b] [B_2 - E]

Ref.a [35, 36], Ref.b [37], Ref.c [38]

3.3. Scanning Electron Microscope (SEM) Images

SEM images of CIGT samples reacted at different ramping rates are shown in Figure 3. It is clearly seen that the ramping rate has a significant effect on the surface morphology of the samples. When the surface image of the sample reacted at 0.5°C/sec was examined, the film surface was seen to have a porous structure. The grain formation started with the increase of the ramping rate and small-grained structure was formed instead of porous structure. In the sample reacting at 5°C/sec, it was formed in large grains with a size of 1-3 µm as well as small grains [39]. When the ramping rate increased to 10°C/sec, it was determined that the surface morphology completely changed, turning into a fused structure [40, 41].

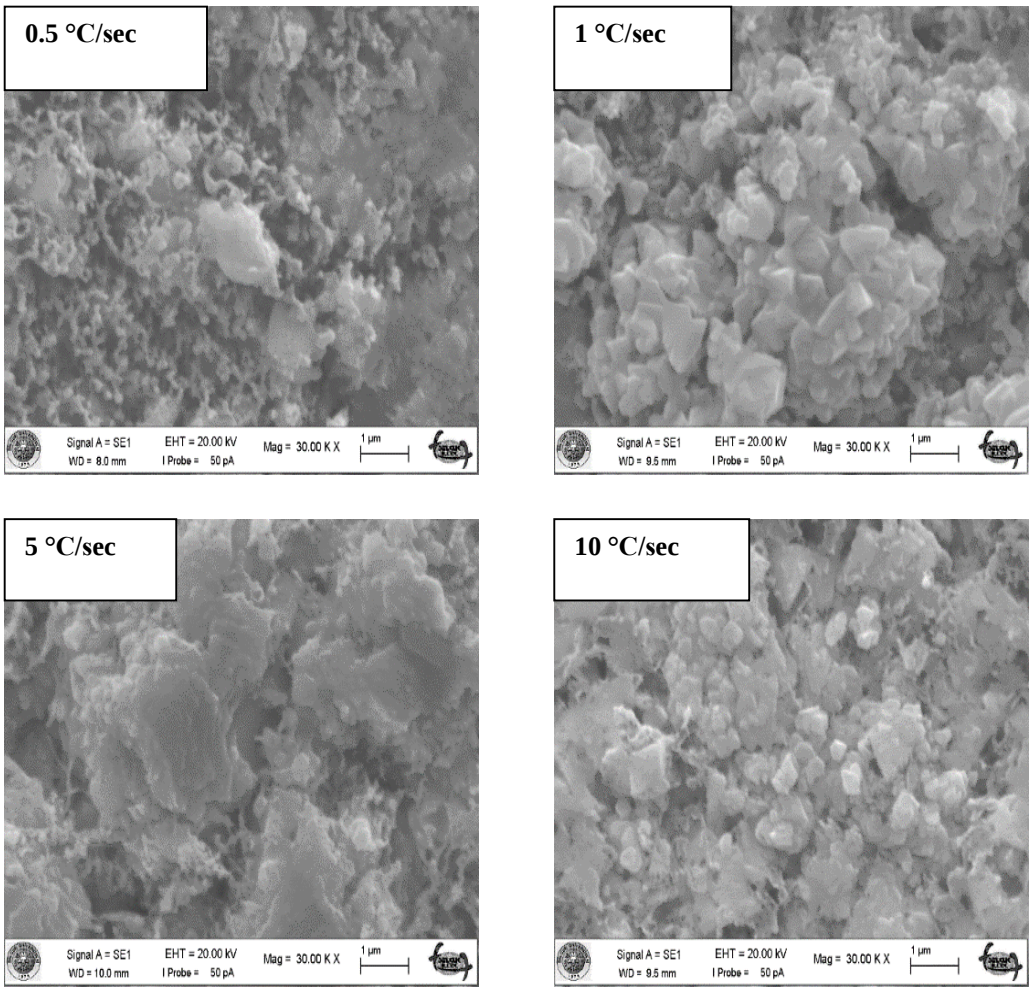

Figure 3 SEM images of CIGT samples reacted at different ramping rates

3.4. Energy Dispersive X-Ray Spectroscopy (EDS) Results

The atomic compositions and the ratios of metallic atoms of CIGT samples reacted at different ramping rates are shown in Table 3. The targeted metallic ratios in the samples are about 0.3 for [Ga]/([Ga]+[In]) and in the range of 0.7-0.9 for [Cu]/([In]+[Ga]). When the table examined, the samples were found to be consistent with the targeted metallic ratios, except for the sample reacting at 0.5°C/sec. In addition, all of the samples regardless of ramping rates were seen to be Te-poor.

Table 3 Atomic compositions and some metallic ratios of the CIGT samples

Elements	0.5 °C/sec	1 °C/sec	5 °C/sec	10 °C/sec
Atomic Compositions				
Cu (%)	17.65	29.91	24.44	22.99
In (%)	27.59	22.51	22.02	20.95
Ga (%)	8.96	13.88	11.10	11.61
Te (%)	45.81	33.69	42.66	44.45
Ratios of Metallic Atoms				
$\frac{(\mathbf{Cu})}{(\mathbf{In})+(\mathbf{Ga})}$	0.48	0.82	0.74	0.71
$\frac{(\mathbf{Ga})}{(\mathbf{In})+(\mathbf{Ga})}$	0.25	0.38	0.34	0.36

4. CONCLUSION

In this study, the effect of reaching the target annealing temperature at different ramping rates on the properties of CIGT thin films was investigated. CIGT thin films were produced by heat treating of foil/Mo/(Cu, In, Ga)/NaF/Te layered structure. In this layered structure, (Cu, In, Ga) precursors were grown by electro-deposition method and then NaF and Te layers were evaporated by electron beam. The annealing process of the samples was carried out with RTP furnace at the target temperature of 600°C for 5 minutes dwell time. To examine the effect of the ramping rate, the target annealing temperature was reached at the ramping rates of 0.5, 1, 5 and 10°C/sec.

XRD results showed that regardless of the ramping rate, all samples crystallized in the chalcopyrite CIGT structure and no secondary phases were formed. Considering the structural parameters such as FWHM and crystallite size of the samples, it was seen that crystal quality improved up to 5°C/sec ramping rate, but started to deteriorate at 10°C/sec. The Raman spectra demonstrated that the CIGT phase was formed at the ramping rates from 0.5 to 5°C/sec, but it was transformed into the CGT phase at 10°C/sec. SEM images showed that the porous structure turned into a large-small grain structure as a result of the increasing of ramping rate from 0.5 to 5°C/sec. However, it was observed that the surface morphology changed and fused structure was formed in the sample reacting at 10°C/sec. The EDS results revealed that the targeted ratios of metallic atoms were achieved, except for the 0.5°C/sec sample, however all samples were Te-poor.

When the characterization results of the samples are evaluated, it can be said that the CIGT absorber layer reacting at 5°C/sec is more suitable for photovoltaic applications.

REFERENCES

[1] Calixto, M., et al., *Compositional and optoelectronic properties of CIS and CIGS thin films formed by electrodeposition.* Solar energy materials and solar cells, 1999. 59(1-2): p. 75-84.

[2] Fernandez, A., et al., *Electrodeposited and selenized (CuInSe$_2$)(CIS) thin films for photovoltaic applications.* Solar Energy Materials and Solar Cells, 1998. 52(3-4): p. 423-431.

[3] Gordillo, G. and C. Calderon, *CIS thin film solar cells with evaporated InSe buffer layers.* Solar energy materials and solar cells, 2003. 77(2): p. 163-173.

[4] Zaretskaya, E., et al., *Raman spectroscopy of $CuInSe_2$ thin films prepared by selenization.* Journal of Physics and Chemistry of Solids, 2003. 64(9-10): p. 1989-1993.
[5] Caballero, R., et al. *CGS-thin films solar cells on transparent back contact*. in *2006 IEEE 4th World Conference on Photovoltaic Energy Conference*. 2006. IEEE.
[6] Ishizuka, S., et al., *Structural tuning of wide-gap chalcopyrite $CuGaSe_2$ thin films and highly efficient solar cells: differences from narrow-gap Cu(In, Ga)Se_2.* Progress in Photovoltaics: Research and Applications, 2014. 22(7): p. 821-829.
[7] Thirumalaisamy, L., et al., *Engineering of sub-band in $CuGaS_2$ thin films via Mo doping by chemical spray pyrolysis route.* Thin Solid Films, 2020. 709: p. 138252.
[8] Aissaoui, O., et al., *Study of flash evaporated $CuIn_{1-x}Ga_xTe_2$ (x= 0, 0.5 and 1) thin films.* Thin Solid Films, 2009. 517(7): p. 2171-2174.
[9] Jung, S., et al., *Effects of Ga contents on properties of CIGS thin films and solar cells fabricated by co-evaporation technique.* Current Applied Physics, 2010. 10(4): p. 990-996.
[10] Li, W., et al., *Fabrication of Cu(In, Ga)Se_2 thin films solar cell by selenization process with Se vapor.* Solar Energy, 2006. 80(2): p. 191-195.
[11] Zhou, D., et al., *Sputtered molybdenum thin films and the application in CIGS solar cells.* Applied Surface Science, 2016. 362: p. 202-209.
[12] Green, M.A., et al., *Solar cell efficiency tables (Version 45).* Progress in photovoltaics: research and applications, 2015. 23(1): p. 1-9.
[13] Kato, T., et al., *Record efficiency for thin-film polycrystalline solar cells up to 22.9% achieved by Cs-treated Cu(In, Ga)(Se, S)$_2$.* IEEE Journal of Photovoltaics, 2018. 9(1): p. 325-330.
[14] Karatay, A., et al., *The effect of Se/Te ratio on transient absorption behavior and nonlinear absorption properties of $CuIn_{0.7}Ga_{0.3}(Se_{1-x}Te_x)_2$ ($0 \leq x \leq 1$) amorphous semiconductor thin films.* Optical Materials, 2017. 73: p. 20-24.
[15] Gremenok, V., et al., *Characterization of polycrystalline Cu(In, Ga)Te_2 thin films prepared by pulsed laser deposition.* Thin Solid Films, 2001. 394(1-2): p. 23-28.
[16] Başol, B.M., et al., *Cu(In, Ga)Se_2 thin films and solar cells prepared by selenization of metallic precursors.* Journal of Vacuum Science & Technology A: Vacuum, Surfaces, and Films, 1996. 14(4): p. 2251-2256.
[17] Witte, W., R. Kniese, and M. Powalla, *Raman investigations of Cu(In, Ga)Se_2 thin films with various copper contents.* Thin Solid Films, 2008. 517(2): p. 867-869.
[18] Witte, W., et al. *Influence of the Ga content on the Mo/Cu(In, Ga)Se_2 interface formation*. in *2006 IEEE 4th World Conference on Photovoltaic Energy Conference*. 2006. IEEE.
[19] Rockett, A., et al., *Na in selenized Cu(In, Ga)Se_2 on Na-containing and Na-free glasses: distribution, grain structure, and device performances.* Thin Solid Films, 2000. 372(1-2): p. 212-217.
[20] Sanad, M., M. Rashad, and A.Y. Shenouda, *Novel $CuIn_{1-x}Ga_xTe_2$ Structures for High Efficiency Photo-electrochemical Solar Cells.* Int. J. Electrochem. Sci, 2016. 11: p. 4337-4351.
[21] Gaburici, D., et al., *Rapid Synthesis of Polycrystalline $CuGa_{1-x}In_xTe_2$ Compounds.* Crystal Research and Technology: Journal of Experimental and Industrial Crystallography, 2000. 35(3): p. 265-270.
[22] Rincón, C., S. Wasim, and G. Marín, *Effect of donor-acceptor defect pairs on the electrical and optical properties of $CuIn_3Te_5$.* Journal of Physics: Condensed Matter, 2002. 14(5): p. 997.
[23] Rincón, C., et al., *Raman spectra of $CuGa_3Te_5$ ordered-defect compound.* physica status solidi (b), 2017. 254(9): p. 1600844.
[24] Rincón, C., et al., *Raman spectra of $CuInTe_2$, $CuIn_3Te_5$, and $CuIn_5Te_8$ ternary compounds.* Journal of Applied Physics, 2000. 88(6): p. 3439-3444.
[25] Rincón, C., et al., *Raman spectra of the chalcopyrite compound $CuGaTe_2$.* Journal of Physics and Chemistry of Solids, 2001. 62(5): p. 847-855.
[26] Rincón, C., et al., *Raman spectra of the chalcopyrite compound $CuGaTe_2$.* Materials Letters, 1999. 38(4): p. 305-307.
[27] Wasim, S., et al., *On the band gap anomaly in I–III–VI_2, I–III_3–VI_5, and I–III_5–VI_8 families of Cu ternaries.* Applied Physics Letters, 2000. 77(1): p. 94-96.
[28] Salem, A., et al., *Synthesis and Electrical Transport Properties of $CuInGaTe_2$.* J Laser Opt Photonics, 2018. 5(183): p. 2.

[29] Chandramohan, M., S. Velumani, and T. Venkatachalam, *Experimental and theoretical investigations of structural and optical properties of CIGS thin films.* Materials Science and Engineering: B, 2010. 174(1-3): p. 205-208.
[30] Badgujar, A.C., S.R. Dhage, and S.V. Joshi, *Process parameter impact on properties of sputtered large-area Mo bilayers for CIGS thin film solar cell applications.* Thin Solid Films, 2015. 589: p. 79-84.
[31] Hsu, W.-H., et al., *Controlling morphology and crystallite size of Cu($In_{0.7}Ga_{0.3}$)Se_2 nano-crystals synthesized using a heating-up method.* Journal of Solid State Chemistry, 2013. 208: p. 1-8.
[32] Atasoy, Y., et al., *Cu(In, Ga)(Se, Te)$_2$ films formed on metal foil substrates by a two-stage process employing electrodeposition and evaporation.* Thin Solid Films, 2018. 649: p. 30-37.
[33] Ananthan, M., B.C. Mohanty, and S. Kasiviswanathan, *Micro-Raman spectroscopy studies of bulk and thin films of $CuInTe_2$.* Semiconductor science and technology, 2009. 24(7): p. 075019.
[34] Ntholeng, N., *Synthesis and characterization of Cu-based telluride semiconductor materials for application in photovoltaic cells*. 2017.
[35] Roy, S., et al., *$CuInTe_2$ thin films synthesized by graphite box annealing of In/Cu/Te stacked elemental layers.* Vacuum, 2002. 65(1): p. 27-37.
[36] Roy, S., et al., *Synthesis of $CuInTe_2$ by rapid thermal annealing of In/Cu/Te stacked elemental layers.* physica status solidi (a), 2002. 189(1): p. 209-221.
[37] Aksu, S., J. Wang, and B.M. Basol, *Electrodeposition of In–Se and Ga–Se thin films for preparation of CIGS solar cells.* Electrochemical and Solid-State Letters, 2009. 12(5): p. D33-D35.
[38] Wasim, S., et al., *Effect of donor–acceptor defect pairs on the crystal structure of In and Ga rich ternary compounds of Cu–In(Ga)–Se(Te) systems.* Journal of Physics and Chemistry of Solids, 2005. 66(11): p. 1990-1993.
[39] Venkatachalam, M., et al., *Investigations on electron beam evaporated Cu($In_{0.85}Ga_{0.15}$)Se_2 thin film solar cells.* Solar Energy, 2009. 83(9): p. 1652-1655.
[40] Fiat, S., et al., *The influence of stoichiometry and annealing temperature on the properties of $CuIn_{0.7}Ga_{0.3}Se_2$ and $CuIn_{0.7}Ga_{0.3}Te_2$ thin films.* Thin Solid Films, 2013. 545: p. 64-70.
[41] Strzhemechny, Y., et al., *Near-surface electronic defects and morphology of $CuIn_{1-x}Ga_xSe_2$.* Journal of Vacuum Science & Technology B: Microelectronics and Nanometer Structures Processing, Measurement, and Phenomena, 2002. 20(6): p. 2441-2448.

Eurasian Journal of Science Engineering and Technology

Research

COMPARISON IN STRENGTHENING OF RCC CONCRETE COLUMN USING FERROCEMENT AND POLYPROPYLENE FIBER ROPE

Al AMIN [1,*], Md. Asaduzzaman PIAL [2], Mahfuz AHMAD [3], Md. Jobaer AHAMED [4]

[1,2,3,4] *Graduate Student, Department of Civil Engineering, University of Asia Pacific, Dhaka, Bangladesh*

ABSTRACT

Extreme loading and severe environmental exposures can cause deterioration of ferroconcrete (RC) columns, this research investigates the performance of external confinement on reinforced concrete short columns subjected to axial loading. Defects, failure and general distress in the structures can be the result of structural deficiency caused by erroneous design, poor workmanship or overloading of the structure. The effectiveness of confinement is achieved by comparing the behavior of retrofitted samples with that of controlled samples. Confining materials are used Ferrocement with wire mesh and polypropylene fiber rope in synthetic rubber adhesive like STAR bond which are easily available. Rectangular short columns having dimension of 150 mm × 150 mm × 900 mm has been cast and tested. The ultimate load carrying capacity for partial confinement (300 mm bottom and top of the column), single layer confinement, double layer confinement with Ferrocement and polypropylene fiber rope confinement are showed to improvement of 31.97%, 56.23%, 59.35% and 30.61% respectively over the control samples. The research results showed that, the confined samples can enhance the ultimate column capacity under concentric loading and improve failure characteristics.

Keywords: Retrofitting, Ferrocement, Confinement, Synthetic adhesive, Polypropylene fiber etc.

1. INTRODUCTION

The retrofit of existing members through external confinement may be a precondition during a seismic redesign strategy aiming at a highly energy-dissipative Ferrocement structure of high ductility. Such a structure could overcome potential overloads by accomplishing full utilization of used materials, sections and member's performance, thus achieving maximum safety for the users. When a concrete column is under axial compression, the interior lateral deformation occurs, leading to cracks. At now the external constraints is employed to supply radial reaction force to concrete, and to confine lateral deformation of concrete tightly. Thus the event of internal micro-cracks is often limited, in order that the development of ductility and compressive strength are often achieved. Consistent with this phenomenon, in engineering projects, the concrete using external lateral restraint to enhance its compressive strength and deformation ability is named confined concrete.

Strengthening the Ferrocement columns may become necessary for variety of reasons, like substandard detailing of the steel reinforcement and deterioration of the concrete under severe environmental conditions [1]. Recent evaluation of the engineering infrastructure has demonstrated that the majority of it'll need major repairs within the near future. Other needs for strengthening arise because either the planning codes have changed that make these structures substandard or larger loads are permitted on the components of the infrastructure where extensive retrofitting is required [2]. Polypropylene is an ultra-high deformability material, widely utilized in the shape of fibers to supply fiber-reinforced concrete with upgraded behavior against plastic shrinkage cracking or spalling of high strength concrete at elevated temperatures [3].

Ferrocement may be a highly versatile sort of ferrocement made from wire mesh, sand, water and cement, which possesses unique qualities of strength and serviceability. It is often constructed with a minimum of skilled labor and utilizes readily available materials. Retrofitting with ferrocement confinement is that the oldest and price effective technique wont to strengthen the concrete structures [4]. Polypropylene fiber ropes made from twisted strands polypropylene fibers provides high lastingness and may be used as an efficient material for strengthening the column and supply higher load carrying capacity. The closely spaced & uniformly distributed reinforcement and use of rich cement mortar provides ductility also as strength, thus improving the load capacity of the retrofitted members. ferrocement also possess some unique properties like waterproofing, fire resistant, low self-weight and sturdy, which makes it a perfect material for wider application. Thus, this research aims to research the general performance of ferrocement and polypropylene fiber rope confinement on normal strength concrete (NSC) reinforced rectangular columns to make sure maximum safety [5, 6].

* Corresponding author, e-mail: alamin.ce18@gmail.com
Recieved: 30.11.2020 Accepted: 19.04.2021

The load carrying ability and ductility of circular concrete columns confined by ferrocement including steel bars (FS) where they're proposed to extend the compressive strength alongside the ductility. The comparative analyses of those models show that the compressive strength of FS columns is improved by 30% than that of BS columns. Thanks to ferrocement caging alongside steel bars samples showed higher ductility, compressive strength and energy absorbing capacity than BS or FRP strengthened circular columns [7].

The utilization of low modulus vinylon and polypropylene fiber ropes as external confining reinforcements on standard concrete cylinders has ultrahigh tensile deformation at failure. The research examined low concrete strength columns in three levels of rope confinement, subjected to monotonic or cyclic loading. The elaboration included that the strain and strain values both at 3% axial strain and at ultimate strain. Suitable fiber rope confinement improved plain concrete strength by an element above 6.6 and provided an axial strain ductility above 40. No column wrapped by polypropylene fiber ropes reached fiber fracture [8].

In this research, the suitability and effectiveness of the ferrocement and polypropylene fiber rope confinement strengthening system to repair RC columns damaged by erroneous design, poor workmanship, overloading are investigated. The particular objectives of the present study are as follows:

1 To investigate the performance of normal strength concrete columns confined by partially, single, double layer ferrocement with wire mesh;
2 To find out the effectiveness of polypropylene fiber rope confinement with on normal strength concrete columns;
3 To compare the effects of confinement to evaluate the ultimate development on load capacities due to different retrofitting techniques.

2. MATERIALS INVESTIGATION

The material properties for binder (Portland cement), fine aggregate (Sylhet sand), and coarse aggregate (stone chips), that is required to calculate the mixture proportions and to maintain homogeneity in mixture proportions are determined according to ASTM (C187, C191, C136, C128, C39) standard procedure for binder, aggregate and reinforcement and also summarized in (Figure 1 and Table 1) are shown below;

a). Coarse Aggregate (stone)

b). Fine Aggregate (sand)

c). Reinforcement (steel)

d). polypropylene fiber rope

e). synthetic rubber adhesive

f). wire mesh

Figure 1. Materials used for research

Table 1. Properties of Materials

Materials	Properties	Unit	Value
Binder (OPC)	Specific gravity		3.15
	Normal consistency	%	27
	Initial setting time	minutes	35
	Final setting time	minutes	338
Fine aggregate	Specific gravity (SSD)		2.54
	Absorption	%	3.35
	Unit Weight	kg/m^3	1628
	Fineness modulus		2.56
Coarse aggregate	Specific gravity (SSD)		2.82
	Void	%	28.90
	Absorption	%	2.02
	Unit Weight	Kg/m^3	1619
	Fineness modulus		4.52
Reinforcement	Yield Strength	MPa	450
	Ultimate Strength	MPa	520

3. METHODOLOGY

To prepare the normal strength concrete according to the ACI-318 standard a suitable mix design ratio is used. The expected compressive strength is 3500 psi after 28 days. Cement: Sand: Coarse Aggregate (1: 1.5: 3), Water: Cement is 0.48, Nominal maximum size of Coarse aggregate 18 mm.

a). Mixing procedure b). Slump test

Figure 2. Preparation of concrete and test of workability

Total samples had been cast with a dimension of 150 mm × 150 mm × 900 mm and a reinforcement ratio of 1.3%. Locally available BSRM 500W bar was used as reinforcing steel (4 nos. 10mm Φ bar @ 4 corners & 6mm Φ bar @ 100mm c/c as tie bars).

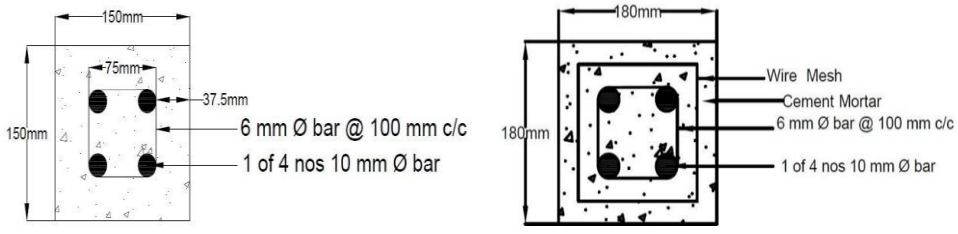

a). Control samples b). Ferrocement with single layer

Figure 3. Sectional view of specimens

The samples are cast into wooden frame as beam. This casting procedure was considered because of the small size of column cross section. Hand compaction was used to compact the concrete with the use of a 16 mm (diameter) tamping rod. Each time the slump value was measured (ASTM C143) and it was between 35 mm – 55 mm. Column samples are demolded after 24 hours of casting.

A rich mortar ratio of cement: sand 1:2 & w/c ratio 0.4 was selected. 80% sample No.16 sieve passing sand is used. The overlapping between the wire mesh layers was 50 mm; the confinement thickness was 15 mm on all sides, making the confined specimen dimension 180 mm × 180 mm × 900 mm for single layer and the confinement thickness was 25 mm on all sides, making the confined specimen dimension 200 mm × 200 mm × 900 mm for double layer of ferrocement with wire mesh. Partially confined where Wire mesh layer is used at top 300 mm and bottom 300 mm height of the specimen, leaving the mid zone unconfined with wire mesh layer. The ferrocement confined samples are further cured for 7 days.

a). Confining with ferrocement b). Confining with ropes c).Confining with Partial ferrocement

Figure 4. Strengthening of different specimens

A locally available synthetic rubber adhesive is used to attach the ropes with the samples. Ropes were attached to the sample with manually applied pull force by hand. Ropes are tightly attached to the surface of the specimens. Samples were tested after 7 days and no special curing technique is used. But the sample were kept in a dry place to keep it away from getting wet in the rain.

4. RESULTS AND DISCUSSION

The ultimate load carrying capacities of both unconfined and confined columns are determined under centric compressive force. The lateral deformations at mid height of the samples are also recorded with an incremental load of 20 kN.

Table 2. The Ultimate load capacity of samples

Sl No.	Types of Specimen	Ultimate Load (kN)	Average load (kN)	% Improvement
01	Control sample	290 298	294	-
02	Partial confinement, C(FP)	395 381	388	31.97
03	Single layer ferrocement, C(FS)	447 454	450.5	53.23
04	Double layer ferrocement, C(FD)	467 470	468.5	59.35
05	Polypropylene fiber rope, C(PER)	385 383	384	30.61

The load vs mid height deflection diagram for all types of samples has been established through averaging the four dial gauge readings. The effect of confinement has been evaluated by comparing the results with unconfined samples. The ultimate load carrying capacity for partial confinement (300 mm bottom and top of the column), single layer confinement, double layer confinement with ferrocement and polypropylene fiber rope confinement are showed to improvement of 31.97%, 56.23%, 59.35% and 30.61% respectively over the control samples. The deflection behavior has been much improved in the confined samples.

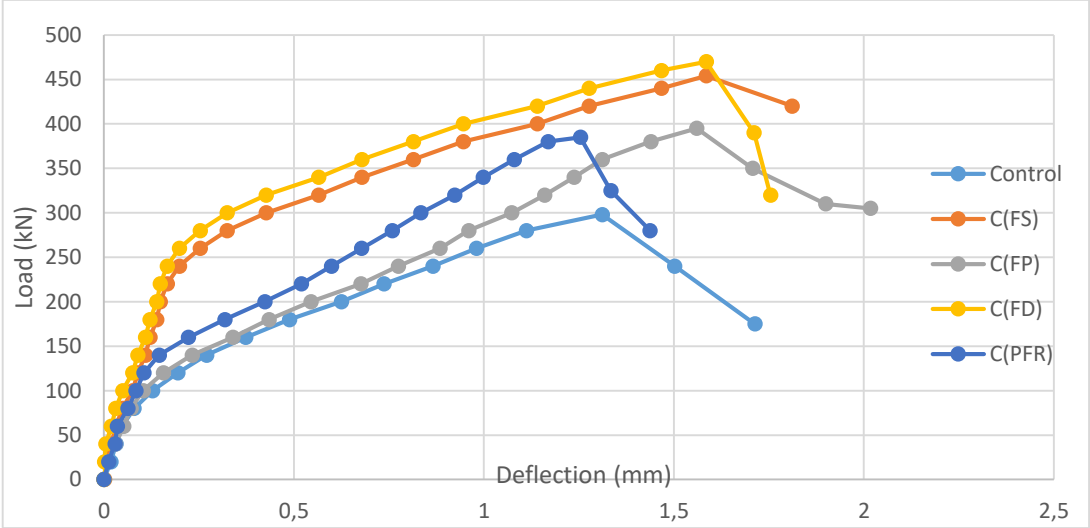

Figure 5. Load vs deflections curve at mid span of different specimens

Initially the deflection in the fully ferrocement confined specimen was less than the unconfined specimen and after the initiation of cracks in ferrocement layers the deflection data gradually increased in the mid-height zone. Compared to the fully confined samples, the partially ferrocement confined samples produced more cracks at mid height due to the absence of wire mesh layer at mid-zone and produced more deflection. The polypropylene fibre rope confined samples showed better results in overall load vs deflection failure mode and showing slightly less deflection than the unconfined samples. All the cases showed slow crack initiation and propagation with respect to the same amount of load over the unconfined samples.

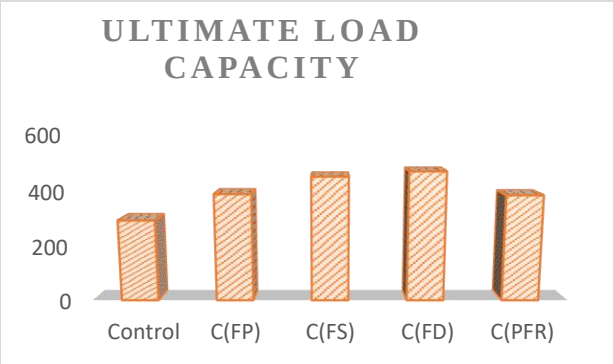

Figure 6. Ultimate load capacity

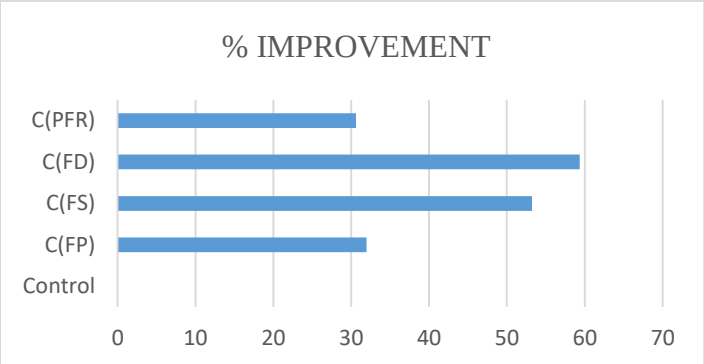

Figure 7. Percentage of improvement

Due to the confinement effect, the deformations first initiated in the ferrocement layers and the core failure took place. In case of fully ferrocement confined (single and double layer) concrete columns, the crack was initiated simultaneously from the base and top of the column. The propagation of cracks was slow due to the presence of thickly populated wire mesh. The crack growth in the fully ferrocement confined samples has been seen mostly at top and bottom along with the edges, but less at mid-height.

a). partially ferrocement confined b). Fully ferrocement confined c). Polypropylene rope layer

Figure 8. Failure mode of specimens

The partially ferrocement confined samples had more crack concentration at mid-height than the fully confined samples due to the absence of wire mesh layer at mid-height. But the edges of the partially confined samples have produced less cracks as the edges had been strengthened with an extra layer of wire mesh.

For the polypropylene rope confinement, the cracks are not visible from outside observation. Cracks initiated in concrete inside the rope layer. At the ultimate load the end crushing type failure became visible and the load readings began to decrease corresponding to the ultimate failure. Rope layer was removed after testing to see the crack pattern in the specimen. The ropes didn't tear off from the surface of the samples as they possess good tensile property and are connected to the specimen with the application of a synthetic rubber adhesive & tension forces.

5. CONCLUSION

The Ultimate load capacities and corresponding behavior of the unconfined and confined (partially, fully & polypropylene fiber rope) columns are determined under the concentric loading condition. External confinement significantly increases the ultimate load capacity of columns & is an effective technique of strengthening to ensure maximum safety. The fully ferrocement confinement showed greater improvement than the partial confinement technique, both in load carrying capacity and slow crack formation, whereas the polypropylene rope confined samples showed slightly less load capacity with a good amount of improvement in mid-height deflection criteria. The ultimate load carrying capacity for partial confinement (300 mm bottom and top of the column), single layer confinement, double layer confinement with Ferrocement and polypropylene fiber rope confinement are showed to improvement of 31.97%, 56.23%, 59.35% and 30.61% respectively over the control samples. The research results showed that, the confined samples can enhance the ultimate column capacity under concentric loading and improve failure characteristics.

6. RECOMMENDATION

The observations and subsequent outcomes of this research project are limited in their scope within the range of a few test variables investigated. It is believed that a wider area in this field is expected and the following recommendations is outlined for future research;

- The performance of confined columns under eccentric and lateral loading and the axial deformation behavior should be investigated.
- Influence of different wire mesh, w/c ratio and support conditions should be investigated.

ACKNOWLEDGEMENT

All praise to almighty. We are grateful to almighty for giving the strength and courage that we are preceding the research with successfully. The preceding of this research involves contribution and assistances from many individuals. Would like to thank all the faculty members of Civil Engineering Department for their support and guidelines. We are also thankful to the support staff and administrative staff who managed so many issues during the work.

REFERENCES

[1] S. T. Smith, and J. G. Teng, "FRP-strengthened RC beams. I: review of debonding strength models," *Engineering structures*, *24*(4), 385-395, 2002.

[2] P. Rochette, and P. Labossiere, "Axial testing of rectangular column models confined with composites," *Journal of Composites for Construction*, 4(3), 129-136, 2000.

[3] A. B. M. A. Kaish, M. R. Alam, M. Jamil, M. F. M. Zain, and M. A. Wahed, "Improved ferrocement jacketing for re-strengthening of square RC short column", *Journal of Construction and Building Materials*; 36, 228–237, 2012.

[4] B. Kondraivendhan, and B. Pradhan, "Effect of ferrocement confinement on behavior of concrete," *Construction and Building Materials*, 23(3), 1218-1222, 2009.

[5] N. M. Apandi, A. Z. Awang, N. J. Hau, L. W. Haur, C. K. Ma, W. Omar, and S. C. S. Yung,"Repair and rehabilitation of concrete structures using confinement: A review," *Journal of Construction and Building Materials*; 133, 502–515, 2017.

[6] T. C. Rousakis, "Elastic Fiber Ropes of Ultrahigh-Extension Capacity in Strengthening of Concrete through Confinement", *Journal of Materials Civil Engineering*; 26:34-44, 2014.

[7] G. J. Xiong, X. Y. Wu, F. F. Li, and Z. Yan, "Load carrying capacity and ductility of circular concrete columns confined by ferrocement including steel bars", *Journal of Construction and Building Materials*; 25, 2263–68, 2011

[8] T. C. Rousakis, "Elastic fiber ropes of ultrahigh-extension capacity in strengthening of concrete through confinement," *Journal of Materials in Civil Engineering*, 26(1), 34-44, 2014.

Eurasian Journal of Science Engineering and Technology

Research

BIOMORPHOLOGICAL, ECOLOGICAL AND ETHOLOGICAL PROPERTIES OF DIPTERA (ARTHROPODA: INSECTA) SPECIES IN DECOMPOSITION PROCESS

Aysel KEKİLLİOĞLU[1, *], Ülkü Nur NAZLIER [2]

[1,2] *Nevşehir Hacı Bektaş Veli University, Faculty of Arts and Sciences. Dept. Of Biology, Nevsehir, Turkey*

ABSTRACT

The existence of insects around the world dates back to 400 million years. People have existed for 300 thousand years. There are more than one million insect species have been identified on earth. The functional properties of insects are examined depending on many different disciplines. Forensic Entomology is the most current of these. The experimental part of this study was conducted between the dates of April 2018 and August 2018 in the Yahyalı locality of Kayseri. Within the scope of the study, Diptera (Arthropoda: Insecta) species, which have a forensic importance, were investigated in terms of their ecological, biomorphological and ethological characteristics. Forensic entomology is the science in which biological information and data related to insect-arthropods are used in cases of misdemeanor and civil lawsuits. The main reason for the use of arthropods in criminal investigations is that they are one of the living species that detect and accept the body as soon as possible, exist in every stage of decay, and some insect species are particularly specific to certain environments and habitats. In the crime scene investigations, the ecology, biomorphology and ethology of insects are used to find out when, how and where the death occurred. Within the scope of the study, in the research conducted; The euthological properties of Diptera individuals in the decomposition process and within the framework of ecological succession were investigated by letting 5 *Rattus rattus* (Linnaeus, 1758) samples per month in the periods are protected. In addition, it is aimed to contribute to forensic entomological researches and analysis of forensic cases by making biomorphological - ecological evaluations.

Keywords: Diptera, Ethology, Ecology, Fauna, Criminology

1. INTRODUCTION

The science that studies insects is called entomology. The existence of insects around the world dates back to 400 million years. There are more than one million insect species have been identified on earth [1-8]. In parallel with their large numbers, ecological diversity is also high for insects.

From the functions specified; Along with the fact that animal carcasses are in the decomposition process, they take part in the clarification of legal processes [6, 7 ,9]. Forensic entomology is the science that investigates the ways and methods of arthropod use in unexpected sudden deaths, unexplained traffic accidents, determining the place and time of death. Forensic entomology refers to a regular decomposition event by predicting the death time by the occurrence of adult individuals who come to the corpse after the death of the living creatures in the Arthropoda branch and Insecta class [1, 5, 10-16]. In forensic entomology science, there is a certain succession of insects that come upon the body. Depending on this temporal succession, the developmental periods of insects are examined and the death time interval (post-mortem interval: PMI) is determined [6, 11, 13, 17, 18] Insects on the body are affected by many variables and perform their colonization accordingly. These variables are meteorological events, the cause and form of death of the corpse, ecological phenomena. [11, 13, 18].

The main reason for the use of arthropodas in forensic events is that they reach the body in a short time and that they are in ecological and periodic succession in the decomposition process make them the most reliable evidence [1, 10, 12, 13, 15, 16].

In the 13th century, Sung Tzu discovered insects by chance to search for the killer of a worker whose throat was cut. He caught the culprit due to the presence of Calliphoridae members in a sickle without blood traces [2, 4, 9, 10, 13, 17-28]. In 1855, Dr. He made the first modern forensic entomological studies by Bergeret. He used S. carnaria's larva as evidence in a courtroom [11, 19, 24-26, 29]. In 2001, Goff proved that forensic insects were the best method in PMI [17, 19, 20, 21, 27, 28, 30-32]. In 2014, Çavuşoğlu detected traces of forensic insects in the decayed human corpses [33].

Ethology is the sub-branch of zoology that studies animal behavior. Ethology encompasses laboratory and field studies carried out in close cooperation with certain disciplines such as evolution, neuroanatomy and ecology [34]. Ethology has been concerned with the basic studies such as revealing the behavioral biology of the species whose environmental conditions are largely shaped by humans, determining the behavioral needs, as well as the development of “biological descriptors” related to

* Corresponding author, e-mail: akekillioğlu@hotmail.com
Recieved: 01.03.2020 Accepted: 01.03.2020
This article is the extended version of the paper that was presented in the UTUFEM Conference 2019.

animal welfare and the examination of the effects of different feeding and feeding conditions on behavior [35]. With the evaluation of ethological features, the position of forensic entomology gains value in legal processes.

Vertebrate animal bodies provide nutrients for many organisms. Insects come at the beginning of these organisms. These form a seasonal and continuous "ecological succession", in which sequential populations colonize and disappear during the decomposition process of the carcass. The timing and nature of succession depends on the size of the carcass, seasonal and environmental climatic conditions and non-biological environmental factors such as soil type. The creatures participating in succession vary depending on whether they are on or in the carcass, just below the carcass or being in the soil near the carcass. At the same time, even in different geographic areas with a similar climate, each succession will also have different species. This is due to the fact that only a few species have a very wide distribution, and therefore each biogeographical region has its own carcass fauna. However, certain taxa that are specialized with carcasses are also determined. [36-40].

The first hierarchy in the decomposition of lechin is the fresh phase (Photo 1.(a).). At this stage, microorganisms and insects that existed in the body begin to decay the body. The second hierarchy begins as the swelling phase (Photo 1.(b).) within a few days. After about 2 weeks, the third stage begins as the active decay stage (Photo 1.(c).), where strong decay odors are formed. At the end of this phase, the carcass becomes almost a dry carcass and only the bones remain in the carcass in response to the fourth stage, the slow dry decay phase (Photo 1.(d).) [17, 27, 40–46].

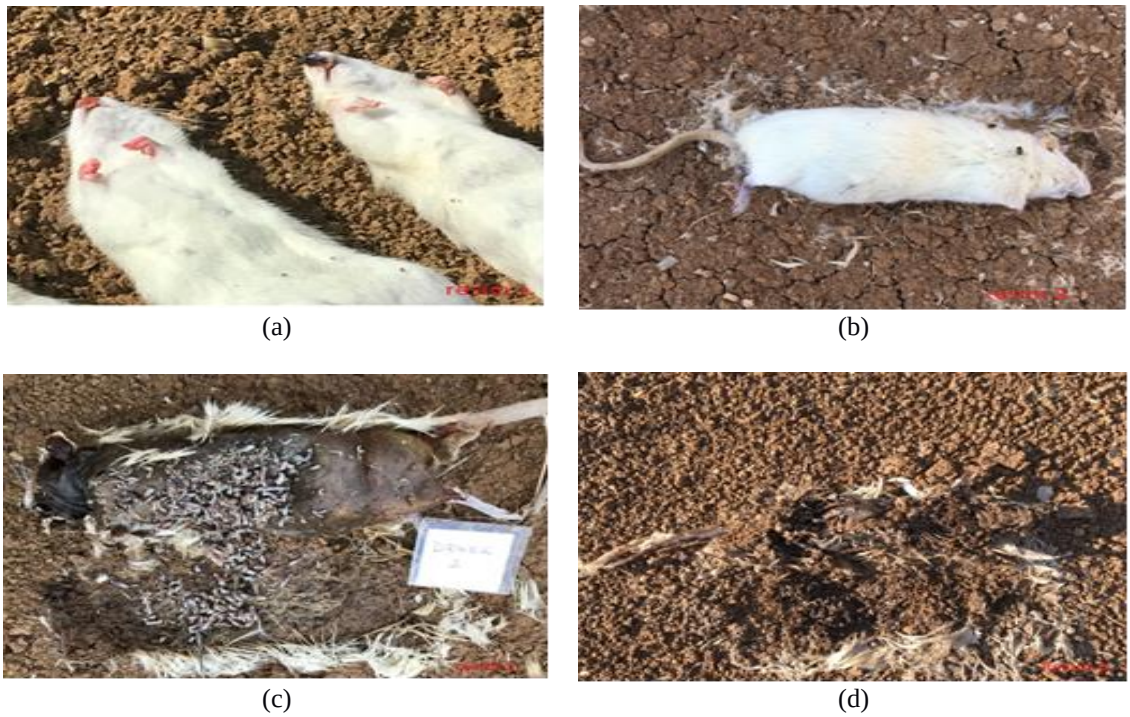

(a) (b)

(c) (d)

Photo 1. (a) Fresh stage, (b) Swelling stage, (c) Decay stage, (d) Drying stage.

Diptera is one of the most populated insect order. They prefer to live in common living spaces with people. They are important in ensuring ecological balance. They are called biplanes. However, while the first pair of wings was found, the second pair of wings turned into a structure called barbell. This transformed structure keeps the Diptera in balance [4, 47, 48]. It is the order that has the best flight ability among insects. There are also wingless types. The layer of the outer kit is not very hard [4]. Adult dipters have sizes between 7 and 10 mm. They can be of various colors. Depending on the antenna types, undercarriages appear. The lower part, whose antennas are long, such as the filiform type, is called nematocera. It is called Brachycera, another subset with its antennae with 3 segments and arista hair at the end [4-7, 17, 28]. The mouth structures are of a licking - absorbent or introducing - absorbent type. They carry two large honeycomb eyes and 3 ocel eyes. They show Holometabol metamorphosis. The larvae are rimless leg type. In the case of the pupa, it is stored in a sheltered place, so as not to prey. They are the fastest species in experimental studies and forensic cases. After death, they reach the body within 1-2 minutes under suitable conditions. They are present in almost all stages of decomposition, except during the drying phase. The reproductive type is ovipar and vivapar. In the case of vivipar, the adult does not lay eggs, but live breeding is in question. Some Diptera species are breeding types when they cannot trust the environment [5-7, 13, 17, 19, 20, 21, 23, 24, 26-28, 47, 48].

2. MATERIAL AND METHOD

Our research covers April 2018 - August 2018. As experimental animals 25 *Rattus rattus* (Linnaeus, 1758), was used for this study. Decomposition length of *Rattus rattus* was taken into consideration to determine our working process. Accordingly, it was determined that the decomposition ended in 30 days by evaluating and observing the ecological environment [10-30,33].

Every month, 5 rats were left by on the experimental land. Daily examinations were made and samples were collected (egg, larval periods, pupa, adult). The skeletons remaining at the end of the month were collected and disposed in appropriate waste units. The ground was ventilated and ground was prepared for new rats. Since we leave the rats on the ground, a special cage arrangement has been prepared and installed to protect it from other factors. Digital temperature and humidity meter were used to measure the ambient temperature. A mercury thermometer was used to measure the temperature of the soil at 10 cm.

Our study was conducted between April and August 2018 in a land where steppe vegetation is observed in Yahyalı locality of Kayseri. It has been used by obtaining the necessary permissions for our land, which is a private property, for easy monitoring of inactive and daily periods away from the residential area. A sheltered area has been chosen so that the land used will not disturb the environment and people. The land is located at a height of 1200 m from the sea at 38 ° 6'36 "N, 35 ° 21'10" D coordinates.

Photo 2. Experiment area

3. RESULTS AND DISCUSSION

3.1. *Calliphora vicina* (Robineau-Desvoidy, 1830)

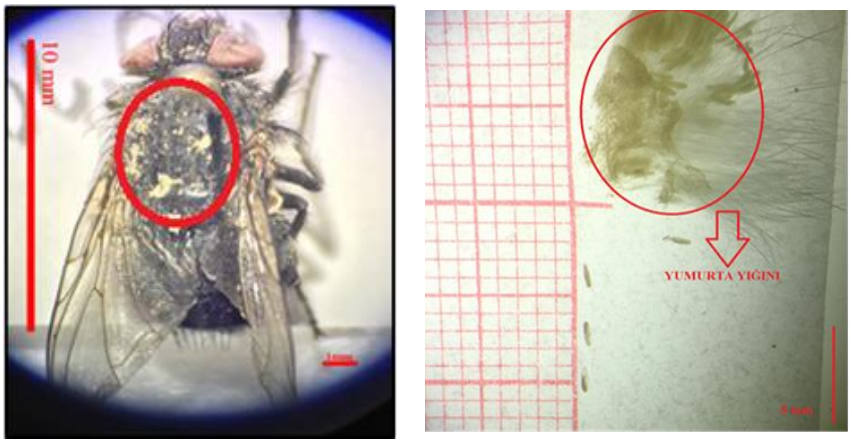

(a) (b)

Photo 3. (a) Dorsal view of *Calliphora vicina, (b)* Egg view belonging to Calliphoridae family

Table 1. Evaluation of *Calliphora vicina* (Robineau-Desvoidy, 1830) [4, 28, 47, 49].

Decomposition	Biomorphology	Ecology	Ethology
Fresh stage Swelling stage Decay stage	Its eggs are 1-2mm in size and adults are 5-13mm in size. Abdomen is metallic blue. Thorax part is dusty blue. The surface of the genea (cheek) part of the head has orange-yellowish black hair. The stem - vein vein on the wing is hairless. The thorax has an acrostical hair pattern.	They can live within 17-25 °C. It is generally seen in spring and autumn seasons.	Migration takes place because the life of the species is forced in a temperature above 25 °C. It has harmonized city life. Due to their biological rhythms, day length is a factor. It has also a relationship with myiasis.

3.2. *Calliphora vomitoria* (Linnaeus, 1758)

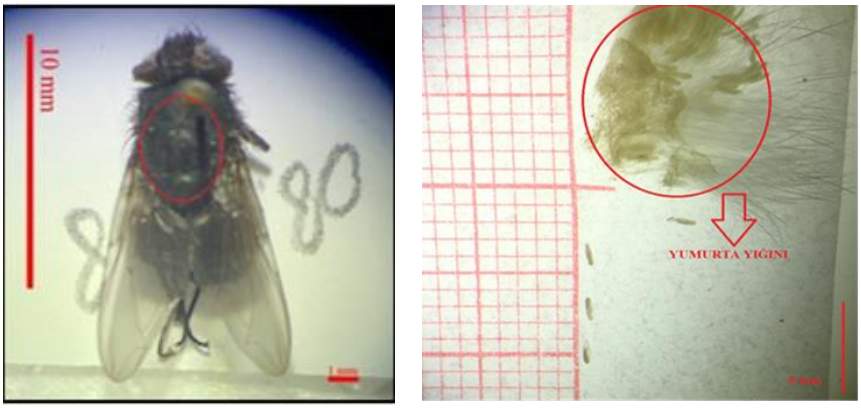

(a) (b)

Photo 4. (a) Dorsal view of *Calliphora vomitoria, (b)* Egg view belonging to Calliphoridae family

Table 2. Evaluation of *Calliphora vomitoria* (Linnaeus, 1758) [4, 28, 47].

Decomposition	Biomorphology	Ecology	Ethology
Fresh stage Swelling stage Decay stage	Its eggs are 1-2mm in size and adults are 5-13mm in size. Abdomen is metallic blue. Thorax part is dusty blue. The genea part of the head part has orange hairs on the black surface. The stem - vein vein on the wing is hairless. The thorax has an acrostical hair pattern	They can live within 15 - 25 °C. It is generally seen in spring and autumn seasons.	Migration takes place because the life of the species is forced in a temperature above 25 °C. They make intense sound while flying. Adapted to rural life. Due to their biological rhythms, day length is a factor. Life activities are active in shade and wooded areas. it has also a relationship with myiasis.

3.3. *Lucilia sericata* (Meigen, 1826)

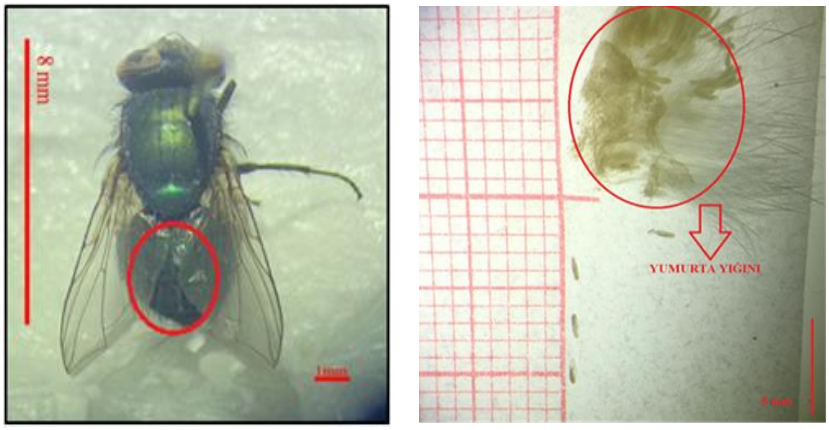

(a) (b)

Photo 5. (a) Dorsal view of *Lucilia sericata*, *(b)* Egg view belonging to Calliphoridae family

Table 3. Evaluation of *Lucilia sericata* (Meigen, 1826) [50, 51]

Decomposition	Biomorphology	Ecology	Ethology
Fresh stage Swelling stage Decay stage	Their eggs are 1-2mm in size, and adults are 5-9mm in size. Abdomen metallic is blue-green. The stem - vein vein on the wing is hairless. 1. The calypter under the double wings is hairless. The basicosta at the point where the wing is attached is yellow in color.	They can experience temperate air within 16 - 27 °C. It is generally seen in spring and autumn seasons.	Flies are the first to come after death. They love fresh carcasses. It is colonized in open and sunny places. It has also a relationship with myiasis.

3.4. *Lucilia cuprina* (Wiedemann, 1830)

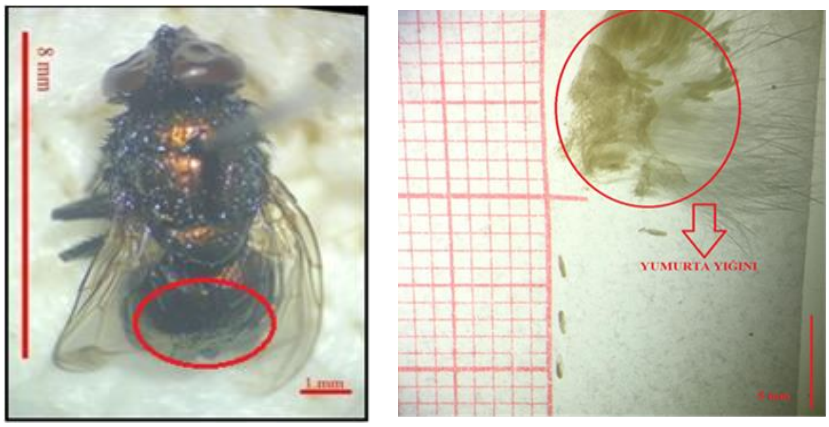

(a) (b)

Photo 6. (a) Dorsal view of *Lucilia cuprina*, *(b)* Egg view belonging to Calliphoridae family

Table 4. Evaluation of *Lucilia cuprina* (Wiedemann, 1830) [4, 52-55]

Decomposition	Biomorphology	Ecology	Ethology
Fresh stage Swelling stage Decay stage	Their eggs are 1-2mm in size, and adults are 5-9mm in size. Abdomen is metallic yellow-copper. The stem - vein vein on the wing is hairless. 1. The calypter under the double wings is hairless. The basicosta at the point where the wing is attached is yellow in color.	They can experience hot air within 17 - 40 ˚C..	Larvae and adults are found on rotten sugar plants, on top of carrion. When they are disturbed, they run away immediately. In a relationship with myazis. They don't enter the houses much.

3.5. *Sarcophaga haemorrhoidalis* (Fallen, 1817)

Photo 7. Dorsal-lateral view of *Sarcophaga haemorrhoidalis*

Table 5. Evaluation of *Sarcophaga haemorrhoidalis* (Fallen, 1817) [28, 56, 57]

Decomposition	Biomorphology	Ecology	Ethology
Fresh stage Swelling stage Decay stage	Adults are 7-14 mm in size. The checkered pattern in the abdomen and the yellow - red in genitalia and the three black bands in the thorax are distinctive points. .	They usually live in shady areas	Adults are fed with liquefied rotten materials. Their larvae feed on carrion and feces. Adults and larvae are vectors. Females give birth to larvae to human carcasses indoors. Its larvae cause myalus. They are the first flies to arrive in the body after heavy rain.

In April, the average temperature value was measured as 12.7 ˚C, humidity 57.8%, soil temperature 5.5 ˚C, and the amount of precipitation was 0.4 kg / m^2. During this month; *Calliphora vicina*, *Calliphora vomitoria*, *Sarcophaga haemorrhoidalis* dominated. The detected species are compatible with the data of Dinar, Topçular, Şabanoğlu and Özdemir [27, 28, 47, 48]. Depending on the temperature data, Calliphoridae larvae shortened the skin change and the process of getting out of the pupa. In this context, there was no difference with the literature [25, 27, 28, 47, 48].

In May, the average temperature value was measured as 15.6 ˚C, humidity 67.6%, soil temperature 6.1 ˚C, and the amount of precipitation as 1.9 kg / m^2. During this month; *Calliphora vicina*, *Calliphora vomitoria*, *Lucilia sericata*, *Lucilia cuprina*, *Sarcophaga haemorrhoidalis* have been identified. The detected species are compatible with the data of Dinar, Topçular, Şabanoğlu and Özdemir [27, 28, 47, 48]. Unlike the previous month, *L. sericata*, *L. cuprina*, was identified. The reason for this was that due to the high density of soil, as a result of the high amount of precipitation during this month, some insects woke up early from sleep and hid in a sheltered area, *Rattus rattus* corpses. Precipitation did not affect the temperature lowering direction. Even the temperature has increased compared to the previous month. Accordingly, *C. vomitoria* reduced her dominance. It has been determined that *L. sericata* is the dominant species. With the effect of rainwater, the corpse was dissolved and skin change times were extended because Calliphoridae larvae could not be fed. Again, with the effect of rain water, the process of entering and exiting the pupa has been prolonged due to the high humidity in the soil. In this context, it contradicts the current literature studies [41, 55, 58].

Average temperature value was measured as 19.1 ˚C, humidity 64.7%, soil temperature 7.8 ˚C, rainfall amount 1.2 kg / m^2 in June. During this month; *Lucilia sericata*, *Lucilia cuprina*, *Sarcophaga haemorrhoidalis* detected. It is in line with the data of Smith, Yuca, Karapazarlıoğlu, Özdemir, Şabanoğlu, Dinar and Topçular [26-29, 47, 48, 55]. Insects are looking for sufficient temperature, humidity and nutrients to breed. *L.sericata*, *L. cuprina* dominated. Depending on the temperature of the calliphoridae larvae, skin change and pupae exit times were shortened. With increasing temperature, *C. vicina* and *C. vomitoria* were not observed. It is also compatible with the current literature [47, 48].

Average temperature value was measured as 22.9 ˚C, humidity 53.1%, soil temperature 9.9 ˚C in July, rainfall amount was 0.1 kg / m^2. During this month; *Lucilia sericata*, *Lucilia cuprina*, *Sarcophaga haemorrhoidalis* were identified. It does not contradict the data of Smith, Çoban, Yuca, Özdemir and Şabanoğlu [17, 27-29,55]. There are species that overlap with our previous 3-month study. *L. sericata*, *L. cuprina* are dominant species. With increasing temperature, the pupae of the Calliphoridae species have shortened their exit time [47, 48].

Average temperature value was measured as 21.9 ˚C, humidity 51.3%, soil temperature 9.5 ˚C, rainfall in 0.1 kg / m^2 in August. During this month; *Lucilia sericata*, *Lucilia cuprina*, *Sarcophaga haemorrhoidalis* were identified. It is in line with the data of Goff, Çoban, Aksoy, Karaazarlıoğlu Özdemir and Şabanoğlu [16, 17, 23, 25-28, 47, 48]. In our study, species overlapping with July were determined. *L. sericata*, *L. cuprina* have been identified as the dominant species. With increasing temperature, the pupae of the Calliphoridae species have shortened their exit time [47, 48].

The first species that came to the *Rattus rattus* corpse were dominant in *C. vicina*, *C. vomitoria*, *L. sericata*, *L. cuprina*, depending on the temperature and humidity. It was observed in the fresh, swelling and decay stages of decomposition. These species are legally important because they perceive the smell of fresh blood immediately. The work done by Şabanoğlu in Ankara coincided with the work done by Özdemir in Ankara [27, 28]. During the 5-month period in which the experimental phase was carried out, *S. haemorrhoidalis* was observed during the fresh, swelling and decay stages. A partial increase in difference was observed in May compared to other months. Because *S. haemorrhoidalis* ideally lived in rainy, closed weather. This behavior made by Şabanoğlu and his current scientific papers was similar [28, 59].

4. CONCLUSION

Depending on the successful evolution of insects, the nutrition, ecology and ethology of each differ from each other. While forensic insects show common characteristics in the field of ecology and nutrition, their ethologies differ depending on ecological factors and rotting natural material. However, they support the contribution to decomposition processes and the development of ecological succession here. These situations play an important role in the elucidation of forensic cases. There are a number of factors that affect forensic entomological examinations. These;

- Geography has different types of insects in different regions.
- Insects have different behaviors.
- While changes in ambient temperature accelerate direct sunlight and high heat succession, sheltered and cold conditions have been found to delay this period.

• Variety, burial or partial burial in situations where the body is exposed in this process significantly slows down the succession process, in this case quite different entomological success. Therefore, in our research, rats have been left in order to obtain more efficient results. The decomposition stages of the species in our study differed (Table 7.).

In our study, Diptera species were observed in fresh and swelling stages. The density of the Coleoptera species have missed the larvae of the Diptera species. The Coleoptera species created a distinction in the decomposition time of the corpse, as they consumed the larvae of the Diptera species.

As a result, it was determined that flies belonging to Calliphoridae and Sarcophagidae families, which are the first wave of decomposition, arrived in the corpse within hours. It was observed that the second and third wave insects arrived in the later stages of the decomposition. These observations are similar to the insect succession sequence made by Smith in 1986 [36]. In 2001, Anderson stated that in addition to the insect succession ranking, insects enter into different behavioral states against ecological factors [60]. In this context; It was also observed that the insects detected within the scope of the study and effective in the decay process deviated from the existing ethological evaluations depending on ecological factors. Anderson (2001) evaluates the occurrence of such situations as normal.

Table 7. Decomposition stages of detected species

Detected species	Decomposition stage detected	Decomposition stage in the literature
***Calliphora vicina* (Robineau-Desvoidy, 1830)**	Fresh, swelling and decay stage	Fresh, swelling and decay stage
***Calliphora vomitoria* (Linnaeus, 1758)**	Fresh, swelling and decay stage	Fresh, swelling and decay stage
***Lucilia sericata* (Meigen, 1826)**	Fresh and swelling stage	Fresh, swelling and decay stage
***Lucilia cuprina* (Wiedemann, 1830)**	Fresh and swelling stage	Fresh, swelling and decay stage
***Sarcophaga haemorrhoidalis* (Fallen, 1817)**	Fresh, swelling and decay stage	Fresh, swelling and decay stage

Decomposition length of Rattus rattus was taken into consideration to determine our working process. Accordingly, it was determined that the decomposition ended in 30 days by evaluating and observing the ecological environment. Velasquez (2007), in his study on *Rattus rattus* in Venezuela, found that the decomposition process was completed in an average of 30 days within ecological factors [61]. Rabbits were used as mammals in the studies of Keskin in 2013 and Başar in 2018. The duration and process of decay of the rabbit was determined by examining ecological factors [25, 62].

Smith (1986) and Anderson (2001) grouped the species identified in the corpse as necrophage, sarcophage, copraphage, dermatophage, predator, parasite and incidental species [36, 60]. In our study, members of Calliphoridae, Sarcophagidae families belonging to the necrophage group were determined. In the studies conducted by Karapazarlıoğlu on buried pig carcass in 2012 and Şabanoğlu - Özdemir on superficial pig carcass in 2007, the insect species and decay stages of Diptera and Coleoptera were similar [26, 27, 28]. In our study, the insect species and decay stages detected on *Rattus rattus* left superficially are in the same direction.

It was determined that *C. vicina*, *C. vomitoria* was active in April and May, and not active in June - July - August. Dinar and Topçular reported that these species live in temperate climates, especially in spring and autumn [47, 48]. Accordingly, our current study data differ from the literature information.

Decomposition stages in forensic entomological studies conducted by Gullan, Ament, Karapazarlıoğlu, Anderson, Goff, Tüzün, Şabanoğlu, Özdemir, Greenberg, Campobassa; It occurs in 4 steps [7, 11, 13, 14, 16, 18, 27, 28, 39, 40]. Within the scope of our study, it was observed that decomposition took place in 4 stages as fresh, swelling, decay and drying stages

ACKNOWLEDGEMENT

I would like to thank Nevşehir Hacı Bektaş Veli University Scientific Research Projects Coordination Unit, which is supported by the Scientific Research Project numbered BAP - YLTPF5.

REFERENCES

[1] H. N. Açıkgöz, İ. H. Hancı, G. Çetin, "Adli olaylarda böceklerden nasıl yararlanırız", *AÜ Hukuk Fakültesi Dergisi*, vol. 51, no. 3, pp. 117–125, 2002.
[2] H. Hancı, "Adli ntomoloji", *Tbb Dergisi*, no. 49, pp. 400-405, 2003.
[3] N. Açıkgöz, "Adli entomoloji", *Türkiye Parazitoloji Dergisi*, vol. 34, no.3, pp. 216 – 221, 2010.
[4] J. H. Byrd and J. L. Castner, *Forensic Entomology: The Utility of Arthropods in Legal Investigations* Boca Raton, Florida: CRC Press, pp. 440, 2001.
[5] M. Kökdener, "Adli entomolojide kullanılan sinek türlerinin Samsun'da mevsimlere göre durumunun belirlenmesi", Doktora Tezi, İstanbul Üniversitesi, İstanbul, pp. 25, 2013.
[6] A. Demirsoy, *Yaşamın Temel Kuralları Entomoloji*. Ankara: Meteksan A.Ş., vol. 2, 1999.
[7] P. J. Gullan, P. S. Cranston, *Böcekler: Entomolojinin Genel Hatları*. Ankara: Nobel Yayın, 2011.
[8] A. Kekillioğlu, "Ankara, Kırıkkale, Kırşehir İlleri Apidae (Insecta: Hymenoptera) türleri üzerine faunistik, sistematik araştırmalar ve bazı ekolojik gözlemler", Doktora Tezi, Ankara Üniversitesi, Ankara, 2005.
[9] A. Özdemir, "Adli entomoloji alanında dünyadan örnekler ve Amerikan hukukunda adli entomoloji uzmanlığı", Doktora Tezi, Hacettepe Üniversitesi, Ankara, 2016.
[10] E. P. Catts, M. L. Goff, "Forensic entomology in criminal investigations", *Annual Reviews of Entomology*, vol. 37, pp. 253-272, 1992.
[11] J. Amendt, R. Kretteck, and R. Zehner, "Forensic entomology", *Naturwissenshaften*, vol.91, pp. 51-65, 2004.
[12] I. R. Dadour, M. L. Harvey, *The use of insects and associated arthropods in legal cases: a historical and practical perspective*‖. Syndney, Australian Academic Pres, pp. 225-32, 2008.
[13] E. Karapazarlıoğlu, "Doğal ortamda domuz karkasları üzerine gelen böcek türlerinin ve süksesyonlarının belirlenmesi ve bir örnek vaka çalışması", Yüksek Lisans Tezi, Ondokuz Mayıs Üniversitesi, Samsun, 2004.
[14] G. S. Anderson, S. L. Van Laerhoven, "Initial studies on insect succession on carrion on southwestern", J. *Forensic Sci*., vol. 41, pp. 617- 625, 1996.
[15] L. M. L. Carvalho, P. J. Thyssen, A. X. Linhares, F. A. B. Palhares, "A cheklist of arthropods associated with pig carrion and human corpes in Southeastern Brazil‖", *Memorias do Instituto Oswaldo Cruz*, vol. 95, pp. 135-138, 2000.
[16] M. Goff, "Entomology‖, encyclopedia of forensic and legal med", *London: Academıc Press*, pp. 263-70, 2005.
[17] E. Çoban, "Edirne Ili Trakya Üniversitesi Güllapoğlu Yerleşkesinde adli entomoloji yönünden önem taşıyan diptera faunasının leş üzerinden toplanması ve taksonomik yönden incelenmesi", Yüksek Lisans Tezi, Trakya Üniversitesi, Edirne, pp. 20-23, 2009.
[18] A. Tüzün, S. Yüksel, "Postmortem intervalin hesaplanmasında adli entomoloji", *Türkiye Klinikleri Dergisi*, vol.4, pp. 23-32, 2007.
[19] S. Selçuk, "Adli entomoloji konusunda jandarma personelinin bilgi düzeyinin değerlendirilmesi", Yüksek Lisans Tezi, Ankara Üniversitesi, Ankara, 2010.
[20] A. Açıkgöz, "İnsan cesetleri üzerinden toplanan entomolojik delillerle ölüm zamanı tayini", Doktora Tezi, Ankara Üniversitesi, Ankara, 2008.
[21] G. Yeşilyurt,"Kırklareli Lüleburgaz Bölgesinde adli entomolojide kullanılan diptera türlerinin tayini", Yüksek Lisans Tezi, İstanbul Üniversitesi, İstanbul, 2011.
[22] M. Benecke, "A brief history of forensic entomology", *Forensic Science International*, vol. 120, pp. 2-14, 2001.
[23] H. Aksoy, "Bazı Calliphoridae (Diptera) türlerinin gelişim aşamaları üzerine çalışmalar", Yüksek Lisans Tezi, Eskişehir Osmangazi Üniversitesi, Eskişehir, 2009.
[24] G. O. Kondakçı, "Adli bilimlerde *lucilia sericata* larvalarının kullanımı", Yüksek Lisans Tezi, İstanbul Üniversitesi, İstanbul, 2009.
[25] S. Keskin, "Kars İli'nde, tavşan (*Oryctolagus cuniculus* L. 1758) cesedi üzerinde zamana bağlı olarak gelişen entomofaunanın belirlenmesi", Yüksek Lisans Tezi, Kafkas Üniversitesi, Kars, 2013.
[26] E. Karapazarlıoğlu, "Samsun İlinde post-mortal dönemde insanda gelişen böcek türlerinin saptanması", Doktora Tezi, Ondokuz Mayıs Üniverstesi, Samsun, 2012.
[27] S. Özdemir, O. Sert, "Determination of coleoptera fauna on carcasses in Ankara Provience, Turkey", *Forensic Science International*, vol. 183, pp. 24-32, 2009.

[28] B. Şabanoglu, O. Sert, "Determination of Calliphoridae (Diptera) fauna and seasonal distribution on carrion in Ankara province", *J Forensic Sci*, vol. 55, no. 4, pp. 1003-1007, 2010.
[29] P. Yuca, "İstanbul, Pendik İlçesi Akfırat Beldesinde adli entomoloji de kullanılan sinek türlerinin belirlenmesi", Yüksek Lisans Tezi, İstanbul Üniversitesi, İstanbul, 2009.
[30] M. Tereli, "Kırıkkale İlin'de tavşan cesetleri üzerine gelen diptera (Arthropoda: Insecta) türlerinin belirlenmesi", Yüksek Lisans Tezi, Kırıkkale Üniversitesi, Kırıkkale, 2011.
[31] M. Wolff, A. Uribe, A. Ortiz, "A preliminary study of forensic entomology in Med. Colombia", *Forensic Science İnternational*, vol. 120, pp. 53- 59, 2001.
[32] N. Açıkgöz, "Adli entomoloji", *Türkiye Parazitoloji Dergisi*, vol. 34, no.3, pp. 217 – 218, 2010.
[33] Y.Y. Çavuşoğlu, "Çürümüş cesetlerin adli entomoloji profillerinin ortaya çıkarılması", Yüksek Lisans Tezi, İstanbul Üniversitesi, İstanbul, 2014.
[34] T. Savaş, İ. Y. Yurtman, "Hayvan davranış bilimi ve zootekni: tanım ve izlem", *Hayvansal Üretim*, vol. 49, no. 2, pp. 36-42, 2008.
[35] D. Smidt, M. C. Schlichting, J. Ladewig, M. Steinhardt, "Ethologische und verhaltensphysiologische forschung für tiergerechte nutztierhaltung" *Arch.Tierz*., vol. 38, pp. 7-19, 1995.
[36] K. G. V. Smith, "A manuel of forensic entomology", *Cornell University Press*, pp. 205, 1986.
[37] D. L. Baumgartner, "Spring season survey of the urban blow flies (Diptera: Calliphoridae) of Chicago, Illinois", *The Great Lakes Entomologist*, vol. 21, pp. 119-121, 1988.
[38] M. L. Goff, "Comparison of insect species associated with decomposing remains recovered inside dwellings and outdoors on the Island of Oahu, Hawaii (Usa)", *Journal of Forensic Sciences*, vol.36, pp. 748-753, 1991.
[39] B. Greenberg, "Nocturnal oviposition behavior of blow flies (Diptera: Calliphoridae)", *Journal of Medical Entomology*, vol. 27, pp. 807-810, 1990.
[40] C. P. Campobasso, G. Di Vella, F. Introna, "Factors affecting decomposition and diptera colonization", *Forensic Sci. Int.*, vol. 120, pp. 18-27, 2001.
[41] M. L. Goff, "A fly for prosecution", *Harvard University Press*, p. 240 , 2000.
[42] J. A. Payne, "A summer carrion study of the baby pig *sus scrofa* Linnaeus", *Ecology*, vol. 46, pp. 592-602, 1965.
[43] M. Wolff, A. Uribe, A. Ortiz, P. Duque, "A preliminary study of forensic entomology in Medellin Colombia", *Forensic Science International*, vol. 120, pp. 53-59, 2001.
[44] L. M. L. Carvalho, P. J. Thyssen, M. L. Goff, A. X. Linhares, "Observations on the succession patterns of necrophagous insects on a pig carcass in an urban area of Southeastern Brazil‖ aggrawal's", *Internet Journal of Forensic Medicine and Toxicology*, vol. 5, no.1, pp. 33-39, 2004.
[45] H. B. Reed, "A study of dog carcass communities in Tennessee, with special references to the insects", *The American Midland Naturalist*, vol. 59, pp. 213-245, 1958.
[46] M. Grassberger, C. Frank, "Initial study of arthropod succession on pig carrion in a central European urban habitat", *J. Med. Entomol*., vol. 41, no. 3, pp. 511-523, 2004.
[47] M. Dinar, "Adli önemi olan böcek türlerinden *calliphora vicina* (robineau-desvoidy, 1830) (Diptera: Calliphoridae)'nın farklı sıcaklıklarda gelişim sürelerinin araştırılması", Yüksek Lisans Tezi, Hacettepe Üniversitesi, Ankara, 2014.
[48] M. Topçular, "Adli önemi olan böcek türlerinden *calliphora vomitoria* (linnaeus, 1758) (Diptera: Calliphoridae)'nın farklı sıcaklıklarda gelişim sürelerinin araştırılması", Yüksek Lisans Tezi, Hacettepe Üniversitesi, Ankara, 2014.
[49] J. Stevens, R. Wall, "Genetic variation in populations of the blowflies *lucilia cuprina* and *lucilia sericata* (Diptera: Calliphoridae). random amplified polymorfic DNA analysis and mitochondrial DNA sequences", *Biochemical Systematics An Ecology*, vol.25, no. 2, pp. 81-87,89-97, 1997.
[50] T. Whiyworth, "Keys to the genera and species of blow flies (Diptera:Calliphoridae) of america North of Mexico‖", *Proc.Entomol.Soc.Wash*., vol. 108, no.3, pp. 689-72, 2006.
[51] T. James, *Flies that cause myiasis in man*. Washington: United States Government Printing Office, vol.4, pp. 1-174, 1947.
[52] P. Catts, N. Haskell, *Entomoloji ve ölüm: bir usul rehberi*. Eng: Joyce's press., 1990.
[53] J. H. Byrd, J. F. Butler, "Sıcaklığın *chrysomya rufifacies* (Diptera: Calliphoridae) gelişimi üzerindeki etkileri", *Tıbbi Entomoloji Dergisi*, vol. 34, pp. 353-358, 1996.
[54] Y. Z. Erzinclioğlu, "Med. veteriner", *Entomo.*, vol. 1, pp.121-125, 1987.
[55] G. V. Smith, "Adli ntomology", *Cornell Üniversitesi Pr, PGS bir Manual*, pp. 1646, 1987.
[56] G. Pekbey, "Türkiye *Sarcophaga* sp. meigen, 1826 türlerinin tanımı ve dağılımı (Diptera: Sarcophagidae)",*Turkısh Journal Of Scıence*, vol.2, no. 1, pp. 15-20, 2017.
[57] A. Durden, "Medical and veterinary entomology", *Academic Press*., pp. 334, 2002.
[58] G. S. Anderson, S. L. Van Laerhoven, "Initial studies on insect succession on carrion in Southwester", *J. Forensic Sci*., vol. 41, pp. 617- 625, 1996.
[59] P. S. Cranton, *The Insects an Outline of Entomology*. New Jersey, U.S.A.: Wiley-Blackwell, pp. 378, 2007.

[60] G. S. Anderson, "Insect succession on carrion and it's relationship to determining time of death",. *Forensic Entomology*: The Utility of Arthropods in Legal İnvestigations, pp. 201- 242, 2001.

[61] Y. Velasquez, "A checklist of arthropods associated with rat carrion in a montane locality of Northern Venezuela", *Forensic Science International*, vol. 174, no. 1, pp. 68-70, 2008.

[62] M. Başar, "Yüzeysel gömülerde adli böcek faunasının tespiti", Yüksek Lisans Tezi, Nevşehir Hacı Bektaş Veli Üniversitesi, Nevşehir, 2018.

Eurasian Journal of Science Engineering and Technology

Research

RESEARCH ON THE ECOLOGICAL SUCCESS ROLE OF THE MUSCIDAE (INSECTA: DIPTERA) SPECIES

Aysel KEKİLLİOĞLU[1, *], Mukaddes BAŞAR [2]

[1,2] *Nevşehir Hacı Bektaş Veli University, Faculty of Arts and Sciences. Dept. of Biology, Nevsehir, Turkey*

ABSTRACT

Since insects are the main dominant group of the Ecosphere, in terms of volume and number; there are many different scientific fields in which insects take place and study. "Forensic entomology" is the most current and interdisciplinary of these fields. Our study aimed to identify individuals belonging to the Muscidae (Insecta: Diptera) family, which has forensic importance within the scope of Nevşehir province. Muscidae species have forensic importance due to their wide distribution, presence in almost every environment and being close to humans. In the decay process, female individuals lay their eggs in natural cavities on the body, open wounds or on bloody clothes. Experiment and application part of the study was carried out in a period of approximately 6 months between April and October 2017. In this study, New Zealand rabbits which were inactive at Ankara University Faculty of Medicine Experimental Animals Laboratory were used. The carcasses are buried in a sheltered area surrounded by wire fences on the land of Nevşehir Hacı Bektaş Veli University. Burying to the soil at a depth of 30 cm was made, in pairs, with and without clothes. On the days determined as 10, 20, 30, 60, 90, 120 and 180, samples were collected from the body. As a result of evaluating the collected samples, 3 species from the Muscidae family, which are involved in the forensic entomological process, in the process of ecological succession, have been identified. These species are*; Musca domestica, Hydrotaea capensis, Stomoxys calcitrans.*

Keywords: Muscidae, Forensic entomology, Ecology, Fauna, Decay, Nevşehir

1. INTRODUCTION

In the case of a suspicious death, the location of the death and the correct determination of PMI (Post Mortem Interval) is very important for justice to be found. The determination of PMI for a body found in the first 24 hours after death can be said by measuring the body temperature precisely [1]. However, in cases where rot begins after the first 36 hours or even after the first 24 hours in hot weather, the sensitivity in determining PMI decreases. Even when the weather conditions are suitable, the margin of error increases in determining PMI. In this case, forensic science makes use of forensic entomology. Forensic entomology can be defined as its use in forensic events by examining insects in many ways, such as their biology, ecology and behavior in determining PMI and place of death in forensic research [2]. Forensic entomology can be defined as the evidence for the use of eggs and larvae of insects or arthropods coming from the corpse in the uncovering of some events from a legal point of view. Forensic entomology is a science that helps forensic medicine or, when it is insufficient, tries to estimate the death time of the victim directly or approximately by the adult and larvae of the insect and other arthropods on the body. Forensic entomology, whose main and most important purpose is to determine the time of death, is also used in uncovering events such as rape, child abuse, non-poisoning, drug and alcohol related deaths, unsolved deaths, smuggling incidents, traffic and aircraft accidents, insurance and inheritance problems. [3]. The most common use of forensic entomology is death. In the post-death period, the information about the death of the victim, the place of killing and whether it is transported can be obtained from the successions and activities of the arthropods [4]. In forensic entomology, insects must first reach the corpses in order to play a role in the decomposition process and to assist the forensic sciences. If a corpse is stored in a place that is completely isolated from its surroundings, or if the corpse is left in an area where the insects cannot survive, the insect may not be found on the body. In these cases, forensic science may not benefit from Forensic Entomology [5]. Insects, which are directly related to human life, also perform the most important step in the decay of their bodies. Insects coming to the bodies in the first step of decay are members of the Diptera ordo that come to the bodies in the first few minutes to start their decomposition period by leaving their eggs or larvae in suitable and sheltered areas of the bodies. The most common Diptera species in forensic entomology belong to the Calliphoridae, Sarcophagidae and Muscidae families. In their study in America, they prepared the morphological features and diagnostic key of the *Calliphora vicina* (Robineau-Desvoidy) and *Phaenicia sericata* (Meigen) species belonging to the periods of eggs, larvae and pupa [6]. Murray Galt Motter et al. systematically studied insects found in more than 150 bodies

* Corresponding author, e-mail: akekillioğlu@hotmail.com
Recieved: 16.06.2020 Accepted: 12.02.2021
This article is the extended version of the paper that was presented in the UTUFEM Conference 2019.

removed from the grave in Washington in the summer of 1896 and 1897. A similar study was carried out in Sweden by the researcher named Schöyen in 1895. The findings of Schöyen were feasible in grave fauna investigations [7]. Eduard Ritter von Niezabitowski, who worked as a medical researcher at the Medico-Legal Institute of Krakau University, used cat, rat, fox, blind rat and calf death in his experiments in May 1899 and September 1900. The priority of Niezabitowski's observations was flies. In his experiments he proved that the arthropods who came to the human body and animal body share the same fauna and made great contributions with the experiments he made in the field of forensic entomology [8]. Medical doctor Marcel Leclercq and Biology Professor Pekka Nuorteva are major researchers interested in forensic entomology from the 1960s to the mid-1980s. Leclercq and Nuorteva are among the first researchers to use forensic entomology in Europe to determine PMI [9]. In our country, the years when studies on the use of insects in forensic entomology came to the fore in the 2000s.These studies, which started primarily with review type researches, mostly continue in the form of graduate thesis studies in provinces such as Ankara, Eskişehir, Edirne, Samsun, etc. [10-22]: Among the researches within this scope, in his research which is an important and preliminary nature; Karapazarlıoğlu determined the insect species on the pig carcass and the succession they form on the carcass with his study in Samsun. Two white pigs were used in the study and it was observed that the pig carcass decomposed in five rotting stages: fresh, swelling, active rot, advanced rot and drying. Also in the decay process; It has been determined that Calliphoridae, Muscidae, Dermestidae, Formicidae, Cleridae, Staphilinidae, Vespidae Piophilidae, Forficulidae species play an active role. Of similar studies; Erzinçlioğlu, by describing the characteristics of the third stage larvae of 10 fly species coming to the meat; Phormia regina, *Phormia terranovae* and *Borellus atriceps* have been described. Current criminal entomology studies in our country are mainly; It is conducted by Sert, Açıkgöz et al., Karapazarlıoğlu, Özdemir, Şabanoğlu, Kökdener, Çoban [10, 12, 16, 18-22].

2. MATERIAL AND METHOD

2.1. Land work

The study was carried out on a land with steppe vegetation in Nevşehir Hacı Bektaş Veli University between April and October 2017. It was used by obtaining the necessary permissions for a land owned by the university. Attention has been paid to ensure that the land used is far from the faculties to the extent that it does not disturb the environment and people. The land is located at coordinates of 38 40 ', 45 "N 34 44', 20" E at an altitude of 1,500 meters from the sea. In our study, 14 New Zealand rabbits were used from the Laboratory of Experimental Animals in the Morphology building of Ankara University Medical Faculty. Necessary permits and documents were obtained for our land use and experiment work. The carcasses are buried in a sheltered area surrounded by wire fences, measuring (20x5) m = 100 m². The experimental area in the study was specially supplied for the study and required wire mesh etc. the hardware was created in accordance with the study. The embedding process with and without clothes was performed in a double group. The study was carried out in approximately 6 months between April and October 2017. The embedded carcasses were each measured in plain white and their weight was 5 kg.

2.2. Laboratory work

The forensic insect fauna, which came to them between April and October 2017, was investigated by embedding rabbits, rabbits with and without clothing at 5 m intervals. During the fieldwork process, ecological parameters affecting the study such as daily temperature, humidity, soil temperature of the area where carcasses are buried were recorded. Accordingly, the relationship between the temperature-humidity-soil temperature of the insects coming to the body was wanted to be revealed. Insect succession on carcasses was investigated on the days determined in the study procedure. In addition, how much the clothing factor affects the decay was examined. Physical changes in each decay phase of the bodies were photographed and recorded. Since the carcasses were buried starting in April, 10, 20, 30, 60, 90, 120, 180 day periods were collected and insect samples in the soil and corpses were collected.

3. RESULTS AND DISCUSSION

During 180 days, a total of 176 adults, about 60 larvae and 25 pupae samples were collected. Three species belonging to the Muscidae family of Diptera have been identified. These species are; *Musca domestica, Hydrotae capensis, Stomoxys calcitrans.* It was observed that these species came to the corpse from the 30th day of burial. It was observed that the months they arrived in the body were June, July and August. In Table 1, given together with the decay phases, removal / inspection times of superficial burials; In Figure 2; daily temperature-humidity-soil temperature graph values of August; has also given.

Figure 1. Decay stages

Table 1. Decay stages

Decay stage	Review Time
Fresh stage	1-30 day
Swelling stage	30-60 day
Active decay phase	60-120 day
Advanced decay stage	120-180 day
Drying phase	180-….day

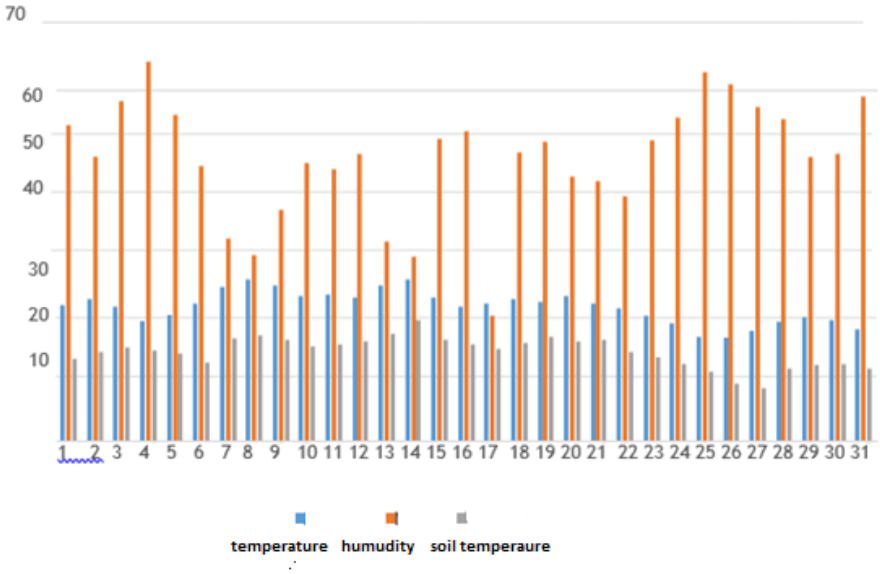

Figure 2. Graph of August temperature -humidity- soil temparature

3.1 *Muscıdae*

It is a family of 4,300 species that is common and known all over the world. Muscidae species have forensic importance due to their wide distribution, being in almost every environment and being close to humans [10].

3.1.1. *Musca domestica,* (Linnaeus, 1758)

Musca domestica Linnaeus 1758, (Housefly), is cosmopolitan, one of the closest living species of diptera. In general, they spread around 3 km of the areas where people are settled. It is not much away from this kind of person and therefore from the dwellings. After garbage, carrion and feces, they cause great trouble because they haunt human food. It is the vector of many pathogens. Adult and larvae prefer stools and spoiled herbal materials. Adults are also attracted by meat and sweet foods, and their larvae can develop sufficiently in these materials [11]. Depending on the temperature, the population reaches its maximum in late Spring and Summer. The rarity of this species on fresh corpse is due to the absence of excrement or intestinal contents [12]. Since they carry a wide variety of disease microbes in their bodies, they infect everything they travel. Because they leave feces to places they visit every 5 minutes. Cholera infects diseases such as diarrhea, dysentery, hepatitis, polio, food poisoning, salmonellosis, tuberculosis [13].

Figure 3. General view of *Musca domestica*

3.1.2. *Hydrotaea capensis* (Wiedemann, 1818)

Figure 4. General view of *Hydrotaea capensis*

It is a cosmopolitan species with a dark metallic gloss and greenish blue color, about 4 - 5.5 mm in length. The palp and antenna are black, calyptras are white or yellowish, the frontal triangle extends to the middle of the forehead and the posterior tibia is slightly curved [14].

3.1.3. *Stomoxys calcitrans,* (Linnaeus, 1758)

Stomoxys flies are blood-sucking obligates, and some species cause significant economic losses in livestock and other warm-blooded animals in many parts of the world. There are 18 species identified so far in the Stomoxys lineage (Diptera: Muscidae). Along with *Stomoxys calcitrans*, which is a cosmopolitan species, other Stomoxys species easily attack pets. Both females and males of Stomoxys flies, which generally show an aggressive and persistent diet, suck blood. Although these flies, which are

also called barn flies, have a wide host variety, rats, guinea pigs, rabbits, monkeys, horses, camels, goats, pelicans and cattle make up their original mansions. Although these flies lead a very active life, they are especially problematic in farms. In addition, they are very important due to their potential to be seen in the settlement areas and beaches close to agricultural production. Severe insertion activities of Stomoxys flies can cause serious problems resulting in milk production and live weight loss. It has been reported to cause losses of 19% in live weight and 40-60% in milk yield [15].

Figure 5. General view of *Stomoxys calcitrans*

3.2. Ecological succession of *muscidae* by dressing factor

Our determinations and evaluations here are given in Table 3.

Table 3. Decay process: In terms of the dressing factor

	DRESSED	**UNDRESSED**
10 th DAY	Eggs were observed in the ear and anus.	Eggs were observed in the ear.
20 th D AY	……..	…….
30 th DAY	*Musca domestica*	*Musca domestica*
60 th DAY	*Musca domestica, Hydrotea capensis*	*Musca domestica*
90 th DAY	*Musca domestica, Stomoxys calcitrans*	*Musca domestica, Stomoxys calcitrans*
120 th DAY	*Musca domestica*	*Musca domestica*
180 th DAY	**……**	**……**

4. CONCLUSION

Table 4. Classification table

PHYLUM	**CLASSIS**	**ORDO**	**FAMILY**	**SPECIES**
ARTHROPODA	INSECTA	DIPTERA	MUSCIDAE	*M. domestica, H. capensis, S. calcitrans*

Forensic entomolog, tries to estimate the time of death of the victim ("corpse") near or approximately, from adult and larvae of insects and other arthropods on the corpse, in cases where it is or is inadequate. is a science. In cases where the moment of death is not known precisely, it is legally important to estimate the time elapsed after death. The most common use of forensic entomology is death. In the post-death period, the information about the death of the victim, the place of killing and whether it is transported can be obtained from the successions and activities of the arthropods [4]. For this purpose, in this study we carried out in Nevşehir, fauna with forensic importance affecting the decay process of the corpse was identified. Since our bodies were buried in the ground and the air temperature was low, the decay process was slow compared to the exposed bodies compared to other studies [16]. The burial of the corpse in the ground will affect the speed of zthe flies reaching the corpse as well as the decay speed. The decay rate of an exposed body can be 4 times higher than the buried corpse. If the soil where the corpse is buried is not very moist and buried deep, the decay rate slows down and the time to stay in the soil increases without degradation.

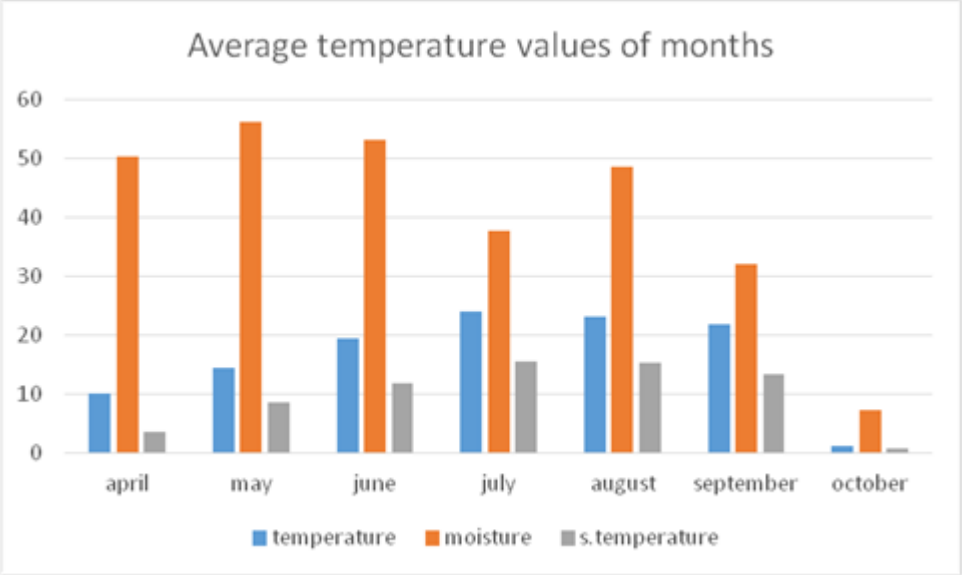

Figure 6. Average temperature values of months

Being buried in the ground negatively affects fly circulation. Buried insects affect the time spent by insects to reach the corpse, the insect sequence, species, and decay stages [17]. No rot or adult insect was found in the bodies during the investigation in the initial phase. The reason for this is that since the beginning of April, the weather is not hot enough, the precipitation is high and the carcasses are buried as frost. During the experiment period, temperature, humidity and soil temperature data covering April 2017-October 2017 were determined. It has been determined that the determined temperature, humidity and soil temperature data and their interactions are the most effective factors in both insect development and rotting. As a result; scope of work; As a result of the burial in the soil at a depth of 30 cm, in pairs and without clothes. On the days determined as 10, 20, 30, 60, 90, 120 and 180, samples were collected from the body. As a result of evaluating the collected samples, 3 species from the Muscidae family, which are involved in the forensic entomological process, in the process of ecological succession, have been identified. These species are; *Musca domestica*, *Hydrotaea capensis*, *Stomoxys calcitrans.* Data obtained from superficial burials with and without clothing were not significantly different in terms of Muscidae faunistic data. However, the outfit; it affects the decay of the corpses, as it provides moisture retention; It has been determined that it accelerates the decay process and stages in balancing conditions parallel to the temperature and soil temperature increase. The rotting process is much more active in the summer months.

REFERENCES

[1] B. Knight and L. Nokes, "Temperature based methods I." in *The Estimation of the Time Scine Death in the Early Postmortem Period*, Arnold, London, 2002, pp: 3- 42.

[2] H. N. Açikgöz, "Adli entomoloji," *Türkiye Parazitoloji Dergisi*, vol. 34(3), pp. 216-221, 2010.

[3] M. Kökdener, "Ölüm zamanı tayininde entomolojik delillerin kullanımı," *Gümüşhane Üniversitesi Sağlık Bilimleri Dergisi*, vol. 5(3), pp. 105-110, 2016.

[4] G. Özer ve F. Önder, "Adli Tıp Olaylarında Böceklerden Yararlanma", *Teknik Bülten : 38*, Tarımsal Uygulama ve Araştırma Merkezi, Ege Üniversitesi, 2001.
[5] J. H. Byrd and J. L. Castner, *Forensic Entomoloyg: Utility of Arthropods in Legal Investigations*, CRC press, Boca Raton, FL. USA, 2000.
[6] Y. Z. Erzinçlioğlu, "The Application of Entomology to Forensic Medicine," *Med Sci Law*., vol. 23(1), pp. 57- 63, 1983.
[7] M. Benecke and R. Lessig, "Child neglect and forensic entomology," *Forensic Science International*, vol. 120, pp. 155–159, 2001.
[8] M. Staerkeby, "Dead larvae of *Cynomya mortuorum* (L.) (Diptera, Calliphoridae) as indicators of the post mortem interval: A case history from Norway," *Forensic Science International*, vol. 120, pp. 77-78, 2001.
[9] W. C. Rodriguez, "The postmortem fate of human remains decomposition of buried and submerged bodies. forensic taphonomy," W. D. Haglund and M. H. Sorg Eds., Florida: CRC Press LLC, 1997, pp. 459-467.
[10] E. Karapazarlıoğlu, "Doğal ortamda domuz karkasları üzerine gelen artropodların ve süksesyonlarının belirlenmesi", Yükek Lisans Tezi, Ondokuz Mayıs Üniversitesi Fen Bilimleri Enstütüsü, Samsun, 2004.
[11] J. I. Coe and W. J. Curan, "Definition and time of death, modern legal psychiatry and forensic science," W. J. Curran, A. L. McGarry and C. S. Petty Eds., Philadelphia: F. A. Davis Co, 1980, pp. 141- 177.
[12] A. Açıkgöz, "İnsan cesetleri üzerinden toplanan entomolojik delillerle ölüm zamanı tayini," Doktora Tezi, Ankara Üniversitesi Sağlık Bilimleri Enstitüsü, 2008.
[13] F. Gregor, R. Rozkosny, M. Bartak and J. Vanhara, "The Muscidae (Diptera) of Central Europe," *Folia Facultatis Scientiarium Naturalium Universitatis Masarykianae Brunensis*, Czech Rep.: Masaryk University, 2002, p. 280.
[14] B. Oğuz, N. Özdal ve S. Değer, "Stomoxys (Diptera, Muscidae) sinekleri ve taşıdığı bazı önemli paraziter hastalıklar," *Kocatepe Veterinary Journal*, vol. 9(2), pp. 97-104, 2016.
[15] C. H. C. Lyal, "The guides to insects of importance to man. 3. Coleoptera. By R. G. Booth, M. L. Cox and R. B. Madge. (Wallingford, CAB International Institute of Entomology, The Natural History Museum, 1990). 384 pp. ISBN 0-85198-678-1. ISSN 0952-1461.," Bulletin of Entomological Research, vol. 81, no. 2, pp. 227–228, 1991.
[16] B. M. Kökdener, "Adli entomolojide kullanılan sinek türlerinin Samsun'da mevsimlere göre durumunun belirlenmesi," Doktora Tezi, İstanbul Üniversitesi, Adli Tıp Enst., İstanbul, 2012.
[17] K. G. V. Smith, "A Manual of Forensic Entomology", *British Museum of Natural History*, London: Cornell University Press, 1986.
[18] P. Yuca, "İstanbul, Pendik ilçesinde Akfırat Beldesi'nde adli entomolojide kullanılan sinek türlerinin belirlenmesi," Yüksek Lisans Tezi, İstanbul Üniversitesi Adli Tıp Enstitüsü, İstanbul, 2009.
[19] E. Çoban, "Edirne ili Trakya Üniversitesi Güllapoğlu Yerleşkesi'nde adli entomoloji yönünden önem taşıyan diptera faunasının leş üzerinden toplanması ve taksonomik yönden incelenmesi," Yüksek Lisans Tezi, Trakya Üniversitesi Fen Bilimleri Enstitüsü, Edirne, 2009.
[20] R. Bana, "Edirne İli Trakya Üniversitesi Güllapoğlu (Balkan) Yerleşkesi'nde adli entomoloji yönünden önem taşıyan coleoptera faunasının leş üzerinden toplanması ve taksonomik yönden incelenmesi",Yüksek Lisans Tezi, Trakya Üniversitesi Fen Bilimleri Enstitüsü, Edirne, 2010.
[21] O. Sert, "Biyokriminal Böcek Bilimi (Entomoloji) Nedir?," *Kebikeç*, vol. 18, pp. 257-259, 2004.
[22] B. Şabanoğlu, "Ankara İli' nde (Merkez İlçe) Leş üzerindeki Calliphoridae (Diptera) faunasının belirlenmesi ve morfolojilerinin sistematik yönden incelenmesi,'' Yüksek Lisans Tezi, Hacettepe Üniversitesi, Fen Bilimleri Enstitüsü, Ankara, 2007.